DE-FC26-03NT41965

Separation of Fischer-Tropsch Wax Products from Ultrafine Iron Catalyst Particles

Technical Progress Report

James K. Neathery, Gary Jacobs, Amitava Sarkar, Adam Crawford, and Burtron H. Davis

Reporting Period
May 1, 2006 to September 30, 2006

The University of Kentucky
Center for Applied Energy Research
2540 Research Park Drive
Lexington, Kentucky 40511-8410

ABSTRACT

In the previous reporting period, modifications were completed for integrating a continuous wax filtration system for a 4 liter slurry bubble column reactor. During the current reporting period, a shakedown of the system was completed. Several problems were encountered with the progressive cavity pump used to circulate the wax/catalyst slurry though the cross-flow filter element and reactor. During the activation of the catalyst with elevated temperature (> 270^{o}C) the elastomer pump stator released sulfur thereby totally deactivating the iron-based catalyst. Difficulties in maintaining an acceptable leak rate from the pump seal and stator housing were also encountered. Consequently, the system leak rate exceeded the expected production rate of wax; therefore, no online filtration could be accomplished.

Work continued regarding the characterization of ultra-fine catalyst structures. The effect of carbidation on the morphology of iron hydroxide oxide particles was the focus of the study during this reporting period. Oxidation of Fe (II) sulfate results in predominantly γ-FeOOH particles which have a rod-shaped (nano-needles) crystalline structure. Carbidation of the prepared γ-FeOOH with CO at atmospheric pressure produced iron carbides with spherical layered structure. HRTEM and EDS analysis revealed that carbidation of γ-FeOOH particles changes the initial nano-needles morphology and generates ultrafine carbide particles with irregular spherical shape.

TABLE OF CONTENTS

EXECUTIVE SUMMARY

In this reporting period, a fundamental filtration study to investigate the separation of Fischer-Tropsch Synthesis (FTS) liquids from iron-based catalyst particles was continued. Catalyst consumption due to filtration losses is a major expense in the operation of slurry phase FTS reactors using iron-based catalysts. Attrition of such catalysts in slurry-phase reactors produces a significant amount of fines, making catalyst separation from the products difficult. During slurry-phase FTS with bubble column reactors, catalysts are generally separated from accumulated reactor wax by either internal filtration or an external system which circulates catalyst back to the reactor. Catalyst fines produced by attrition may cause filters to plug and are difficult to separate by settling. As a result, multiple filtration stages are needed in order for the waxes to be well-suited for down-stream processing.

The overall objective of this filtration study is to test the effectiveness of various crossflow filtration procedures with simulant FTS slurry. The wax products from a FTS reactor can vary widely depending on the type of process implemented. In this study, the focus is on high-alpha iron-based slurry-phase reaction processes. The change in filtration properties of iron catalyst slurries will be correlated with physical and chemical changes of the particles during Fischer-Tropsch conditions.

Phase-transformation of iron catalyst during activation/FTS plays an important role in determining the structural integrity or attrition resistance of the catalyst particles. Sequential phase-modification during the activation process (with CO or synthesis gas) from hematite to magnetite and finally to iron carbides have been reported. The chemical conversion of iron oxides to iron carbide induce a volumetric change because of significant difference in the skeletal densities of carbide and oxide structures (e.g., 7.7 g cm^{-3} for Fe_3C as compared to 5.2 g cm^{-3} for Fe_3O_4). The volumetric change can cause stress in the particle which can lead to attrition and formation of small crystallites of iron carbides that split off rapidly to form ultrafine particles. Physical attrition can also result from collision between catalyst particles and the reactor internals.

The effect of carbidation on the morphology of iron nano-needles have been examined in the absence of any mechanical stirring in the present study. Homogeneous oxidation of Fe(II) results in the precipitation of ultrafine $\gamma - FeOOH$ particles having a needle-like structure. Carbidation of $\gamma - FeOOH$ with CO at atmospheric pressure and 270 °C temperature transform the oxide phase to multicrystalline carbide phase. Electron microscopy imaging study revealed that carbidation caused the disapprearance of the initial needle-like morphology of the particles and generates small crystallites of irregular shaped sphere. Volumetric stress generated during the carbidation process might be responsible for the fragmentation of the nano-needle structures.

Used catalyst samples, representative of onstream Fischer-Tropsch synthesis conditions, were retrieved from the CSTR reactor and solidified in the waxy matrix. XANES spectra recorded at the K-edge indicated that the alkali promoter used, rubidium, was in an oxidized state and that the compound most prevalent in the used catalyst samples closely resembled reference spectra for Rb carbonate.

In the current reporting period, work has ended to modify the CAER's 4 liter bubble column reactor to include the FT wax filtration scheme developed during the previous Phase of this research program. In the modified reactor system, a moyno-type progressive cavity pump was included to convert the reactor from a natural to forced circulation liquid circuit. The wax/catalyst slurry will have two separate flow paths: 1. a low flow circuit (1-2 lpm) passing through the bubble column, and 2. a higher rate slurry path through the cross-flow filter. Several problems with the circulation pump were encountered. The pump seal initially was unable to provide an acceptable leak rate under the operating synthesis pressure. Additionally, the elastomers of the pump stator were not compatible with the FT slurry during the elevated temperatures needed for catalyst activation. Breakdown of the elastomer released sulfur which quickly deactivated the iron catalyst.

In order to test the proposed filtration under real-world conditions it was decided to operate the filtration system independent of the SBCR pilot system. In lieu of FT wax produced directly from the bubble column, we prepared a test slurry containing FT wax rendered from previous pilot SBCR and CSTR reactor tests and activated ulrafine Mach I iron catalyst (0.26 wt% as Fe). The goal of this test was to monitor and record filter flux measurements over a long term time on stream period (500+ hours). Various flux maintenance or filter cleaning procedures were employed over the long term test, attempting to stabilize the flux over time.

TASK 1. Fundamental Filtration Studies

Task 1.1 Shakedown *(subtask completed)*

Task 1.2. Solvent wax experiments *(subtask completed)*

Task 1.3. Filtration studies with doping of olefins and alcohols *(subtask completed)*

Task 1.4. Ultra-fine Iron Filtration

Precipitated Iron Fischer-Tropsch Catalyst: Effect of CO activation on the Morphology of Iron Hydroxide Oxide Nanoneedles.

1. Introduction

Iron oxyhydroxides ($\alpha-FeOOH$, $\gamma-FeOOH$ or $\delta-FeOOH$) are used extensively as catalysts, co-catalysts, pigments, flocculents, etc. [1-5]. The oxidation of $Fe(OH)_2$ in aqueous solution can produce Fe_3O_4, $\alpha-FeOOH$ or $\gamma-FeOOH$ depending on the reaction temperature, oxidation rate, initial concentration of the reactants and pH of the medium. Fast oxidation produces $\gamma-FeOOH$ while slow oxidation results in the formation of Fe_3O_4. The formation of $\gamma-FeOOH$ is restricted to the instances where the rapid aerial oxidation of ferrous ion is effected in a neutral or slightly basic suspension of $Fe(OH)_2$. However, $\gamma-FeOOH$ is not formed by the addition of a base to effect precipitation of iron from a solution prepared from a ferric salt [6].

$\gamma-FeOOH$ has been used extensively as an active catalyst for Fischer-Tropsch synthesis [6,7], for recovering useful hydrocarbons from palm shell oil [1], oxidation of benzoic acid by hydrogen peroxide [2], and for direct liquefaction of coal [4]. The oxidation of $Fe(OH)_2$ and the mechanism of formation of $\gamma-FeOOH$ was studied extensively [8,9]. Electron microscopy analysis of the samples withdrawn at different times of oxidation/precipitation reaction revealed a pattern of changes in the particle morphology during the formation of $\gamma-FeOOH$. The initial shapeless material transformed to needle-type structure of $\gamma-FeOOH$ particles via the formation of different dense spherical and hexagonal structures.

Application of in situ Mössbauer spectroscopy recorded during Fischer-Tropsch synthesis showed that the level of CO conversion increases with the formation of iron carbides, i.e., $\varepsilon'-Fe_{2.2}C$ and $\chi-Fe_{2.5}C$ [7]. Sequential phase-modification during the activation process (with CO or syngas) from hematite to magnetite and finally to iron carbides have been reported [10-12]. Phase-transformations during activation/FTS may play an important role in determining the structural integrity or attrition resistance of the catalyst particles. Although the transformation of amorphous $Fe(OH)_2$ to $\gamma-FeOOH$ and related structural details were studied extensively, those of the transformation of $\gamma-FeOOH$ to iron carbides upon CO activation are not yet reported in the literature. The objective of the present research is to investigate the structural transformation of $\gamma-FeOOH$ nano-needles upon carbidation with CO. Ultrafine $\gamma-FeOOH$ was prepared by oxidation of $Fe(OH)_2$ and the change in particle morphology was monitored by HRTEM imaging.

2. Experimental

2.1 Preparation and carbidation

$FeSO_4 \cdot 7H_2O$ (ACS reagent, $\geq 99.0\%$, 215422), NaOH (ACS reagent, $\geq 97.0\%$, pellets, 221465), and $BaCl_2 \cdot 2H_2O$ (ACS reagent, $\geq 99.0\%$, 217565) were purchased from Aldrich, Inc. and were stored in a desiccator to prevent deterioration. 99.99% O_2 (UHP grade, AGA Speciality Gas) and deionized water was used for the preparation of $\gamma-FeOOH$. For the carbidation of $\gamma-FeOOH$, 99.99% CO (UHP grade, AGA Speciality Gas) was used and C-30 oil (hydrogenated polyalphaoleffins, CAS# 68037-01-4) was used as start-up solvent.

For the preparation of $\gamma-FeOOH$, a four-neck round-bottom flask (1 L) was used. The flask was fitted with a gas dispenser (fritted glass disc), pH electrode, motor driven stirrer, and gas inlet/outlet tubes. Inlet gas flow rate was monitored by a pre-calibrated mass flow controller and the outlet gas flow rate was monitored by a wet-test flowmeter. The reaction flask was placed in a constant temperature water bath maintained at 25 °C. The carbidation of $\gamma-FeOOH$ was performed in a glass cylinder (50.8 mm ID) fitted with fritted glass disc at bottom. The gas inlet and outlet lines were fitted with valves. The inlet gas passed through the fritted glass disc and bubbled upward through the slurry (C-30 oil and suspended $\gamma-FeOOH$ particles) keeping the suspension stirred. In order to avoid the possibility of breakage of initial needle-type structure of $\gamma-FeOOH$ particles, any kind of mechanical stirring was avoided. The cylinder was wrapped with heating tape and a thermocouple placed outside to monitor the skin temperature of the cylinder. The skin temperature was controlled by a temperature controller (CN3251-R, Omega, Inc.).

For the preparation of $\gamma-FeOOH$, 750 mL of deionized water was added to a 1 L round-bottom flask and nitrogen gas was bubbled through the water (stirred at 800 rpm) for 45 minutes to remove any dissolved carbon dioxide and oxygen, and then 41.7 g of $FeSO_4 \cdot 7H_2O$ was added. After 10 minutes, solid NaOH (10.3 g) was added to maintain a molar ratio of $[Fe(II)/[OH^{-1}]]$ of 0.5833 (= 7/12). The suspension was stirred for 15 minutes under nitrogen at room temperature until the suspension pH became constant. Oxygen was then passed into the solution at a constant rate of 18.5 cm^3 min^{-1}. Reaction time was measured from the start of oxygen flow. During the reaction, the pH value was recorded every minute. The extent of the oxidation reaction was easily recognized from a comparison of the outlet and inlet flow rate of oxygen, the pH and color of the

suspension. After 1 h the oxidation had essentially stopped. The product was then collected by filtration and then washed with deionized water several times until SO_4^{2-} was not detected in the filtrate. A $BaCl_2$ solution was used to test for the presence of SO_4^{2-}. The filter cake was then washed with acetone to remove most of the water. The precipitate was dried in vacuum at room temperature for 24 h.

Carbidation of the prepared $\gamma - FeOOH$ (i.e., activation with CO) was performed at atmospheric pressure using C-30 oil as the solvent. The $\gamma - FeOOH$ loading of the slurry was 5 wt%. The CO flow rate (3.0 sl/h/g Fe) was controlled by a pre-calibrated mass flow controller. The temperature of the slurry was raised from 25 °C to 270 °C with a ramp rate of 1 °C min^{-1}. The flow rate of the exit gas was measured using a digital bubble flow meter and the composition was analyzed by a micro GC equipped with thermal conductivity detectors. At the end of the carbidation, the slurry sample was withdrawn and stored under C-30 oil in a desiccator maintained at vacuum.

2.2 Characterization

The X-ray diffraction pattern of the product was measured using Cu Kα (1.5418 Å) radiation (40 kV and 20 mA) with a Philips x-ray diffractometer. For analysis by X-ray diffraction, the solid sample was ground and placed in a sample holder in a glovebox. The sample was removed from the glovebox immediately prior to the measurement.

The slurry samples were diluted with hot (about 70°C) o-xylene to remove the C-30 oil. Although it was not possible to completely remove the C-30 oil by this method, the leftover oil did not interfere with TEM analysis and acted as a protective cover for the air-sensitive carbide particles. An optimum ratio of o-xylene to particles was used to

make a slightly turbid suspension for TEM analysis. A drop of the suspension was placed onto a lacey carbon film on 200 mesh copper grid and loaded into the microscope.

The particle morphology was analyzed by a field emission analytical transmission electron microscope (JEOL JEM-2010F) operated at an accelerating voltage of 200 kV and equipped with a STEM unit with high-angle annular dark field (HAADF) detector, and a Gatan Imaging Filter (GIF)/PEELS system. The electron beam had a point-to-point resolution of 0.2 nm. Gatan Digital Micrograph® software was used for image processing.

3. Results and Discussions

A white precipitate was formed when $FeSO_4$ and NaOH were mixed in a ratio that produced a suspension with an initial pH of 8.3. In the present experiment, the molar ratio of $[Fe(II)/[OH^-]]$ was 0.5833 (7/12). Under this condition, essentially all of the added OH^- ions are consumed to form $Fe(OH)_2$, and (1/7)th of the Fe(II) remains in solution. Because the added base is consumed in the precipitation process, the suspension is only slightly basic (pH = 8.3). Thus the initial reaction can be described as follows:

$$7FeSO_4 + 12NaOH \rightarrow 6Fe(OH)_2 + 6Na_2SO_4 + Fe(II) + SO_4^{2-}$$

As oxygen is passed through the suspension, the white precipitate was oxidized and the color of the mixture turned first to green, then blue, and finally orange-yellow. The change in pH with reaction time during the oxidation process is presented in Figure 1. Several distinct stages can be observed. During the first stage, the pH of the suspension was reduced from 8.3 to about 7.9. At the end of this stage, the pH abruptly decreased to about 6.4 during 5-6 minutes with continuous oxygen flow. This sharp drop in pH is due to oxidation of Fe(II) by oxygen and the hydrolysis reactions of the oxidation species [6]. During the next stage of oxidation, the pH remained constant about 6.2. As with the first

stage, there was finally an abrupt decrease in pH to about 4 following which the oxygen consumption became very low and the pH remained nearly constant.

During the initial course of oxidation, ferrous ions in the solution are oxidized to produce ferric ions which combine with ferrous ions to form an iron mixed-valence green complex. It has been reported that the green complex consists of Fe(II)-O-Fe(III) [13] which oxidized further to produce $\gamma - \mathrm{FeOOH}$ during the second stage. It was calculated that at the end of first stage, $\mathrm{Fe(OH)_2}$ completely converts to green rust and the molar fraction of Fe(III) in the green rust was estimated to about 30% [6]. Electron microscopy studies revealed that the initial amorphous material developed to form green rust with morphology of large thin hexagonal crystals which contains holes. With the initial, sudden pH decrease at about 33% conversion of the total amount of Fe^{2+} that is oxidized, small, dense, hexagonal Fe_3O_4 particles were formed in addition to the green rust hexagonal crystals. The disappearance of Fe_3O_4 and green rust particles with further oxidation was accompanied by the development of needle-type $\gamma - \mathrm{FeOOH}$ particles [8]. A reaction sequence as described by David [6] representing the oxidation pathway from $\mathrm{Fe(OH)_2}$ to $\gamma - \mathrm{FeOOH}$ is presented in Figure 2. The X-ray diffraction pattern of the final synthesized product is shown in Figure 3 which confirms that the final oxidation product contains $\gamma - \mathrm{FeOOH}$ and only traces amount of $\alpha - \mathrm{FeOOH}$.

The HRTEM pictures of the synthesized $\gamma - \mathrm{FeOOH}$ particles are shown in Figure 4a-4f. The HRTEM images confirm that only fiber particles of $\gamma - \mathrm{FeOOH}$ are present and the final oxidation product does not contain any other particle morphology such as hexagonal or spherical particles. The average length of the rod-shaped particles (nano-

needles) are 150-200 nm and average particle diameter is about 5-10 nm. The crystalline needle-shaped particles have a three dimensional network with a characteristic d-spacing of 2.5 Å (corresponds to [031] plane of $\gamma - FeOOH$). An electron microdiffraction pattern of synthesized particle is shown in Figure 5. The typical electron diffraction pattern obtained from this sample together with the x-ray diffraction pattern confirms the presence of $\gamma - FeOOH$ as the predominant phase [6].

Analysis of the outlet gas during CO activation revealed the amount of CO_2 generated during the carbidation is represented in Figure 6 (mol of CO_2 per g of iron against time). The first peak of this profile (around 3.75 h) corresponds to the quick transformation of $\gamma - FeOOH$ to Fe_3O_4. The second and broad peak (starting around 6 h) corresponds to the slow transformation of Fe_3O_4 to iron carbides which continue up to around 10 hours. After this period, the amounts of CO_2 produce start to decline quickly.

The morphology and chemical nature of the CO activated particles were examined by HRTEM, EDS and electron-microdiffraction techniques. The HRTEM images of the carbided particles are shown in Figure 7a-7f. The change in the morphology of the particles is evident. The initial needle-type structures of the $\gamma - FeOOH$ particles have disappeared almost completely upon carbidation. Formation of ultrafine crystalline circular shaped structures can be noticed. These small crystallites (irregular shaped sphere) are multicrystalline in nature as evident from electron diffraction pattern shown in Figure 8. The non-smoothed and non-perfect spherical particles (Figure 7c and 7e) have a crumpled and boulder-like appearance. These structures originate from nanocrystalline grains within and on the nanoparticle surface. The carbide particles are made of aggregates of nanocrystals. The higher resolution images (Figure 7e and 7f)

shows atomic plane zones indicating crystalline grains in the particles. The characteristic d-spacing of these crystallites is 2.1 Å (can corresponds to [510] plane of $\chi - Fe_5C_2$, [111] or [101] plane of $\varepsilon' - Fe_{2.2}C$), [210] or [111] plane of $\varepsilon - Fe_2C$).

The EDS analysis of the CO activated sample shown in Figure 9 also confirmed the transformation of the oxide phase to carbide phase. The elemental compositions of the activated particles are shown in Table 1. Presence of small amount of oxygen suggests that the transformation of oxide to carbide phase was not complete. It is difficult to reach full conversion in the oxide-carbide transformation. It has been reported that CO activation of ultrafine iron oxide at 270 °C and atmospheric pressure for 24 h results in 85% carbide only [14]. Hence, it is unlikely to convert $\gamma - FeOOH$ particles to iron carbides completely by 10-12 h. The leftover oxide core may remain under the carbide phase with a layered structure.

Oxide-carbide phase-transformations during activation and/or Fischer-Tropsch synthesis play an important role to determine catalytic activity and attrition resistance of the particles. The chemical conversion of iron oxide phase to iron carbide phase induce a volumetric change due to significant difference in densities and the resulting shear lead to formation of small crystallites of iron carbides which split off rapidly to form ultrafine particles [15]. The conversion of oxide to carbide phase is dynamic and reversible depending upon the environment.

It was reported that while using iron oxide particles of 100-200 micron in size for FTS, the carbide phase forms as small nodules on the surface of the magnetite and the phase transformation proceeds slowly into the bulk [11]. The volumetric change during the oxide to carbide transformation results the sprouting of carbide buds/nodules on the

surface of magnetite crystal. However, such phenomena were not observed in the present study using particles that are much smaller, at least in two of their dimensions. The carbide particles were identified as bulk phase with layers. The transformation of carbide phase results in the loss of the initial needle-like structure of $\gamma - FeOOH$. Since any kind of mechanical stirring was avoided during the carbidation process, this change of morphology is due to change in chemical nature of the particles only.

4. Conclusions

Homogeneous oxidation of Fe(II) results in the precipitation of ultrafine $\gamma - FeOOH$ particles having a needle-like structure. Carbidation of $\gamma - FeOOH$ with CO at atmospheric pressure and 270°C temperature transform the oxide phase to multicrystalline carbide phase. Electron microscopy imaging study revealed that carbidation caused the disappearance of the initial needle-like morphology of the particles and generates small crystallites of irregular shaped sphere. Volumetric stress generated during the carbidation process might be responsible for the fragmentation of the nano-needle structures.

References

1. T. Masuda, Y. Kondo, M. Miwa, T. Shimotori, S. R. Mukai, K. Hashimoto, M. Takano, S. Kawasaki, S. Yoshida, Chemical Engineering Science, 56 (2001), 897-904.
2. S. Chou, C. Huang, Y. H. Huang, Environmental Science and Technology, 35 (2001), 1247-1251.
3. S. Chou, C. Huang, C., Chemosphere, 38(1999), 2719-2731.

4. T. Kaneko, K. Tazawa, N. Okuyama, M. Tamura, and K. Shimasaki, Fuel, 79 (2000), 263-271.
5. K. Asami, Y. Ohtsuka, Industrial & Engineering Chemistry Research, 32 (1993), 1631-1636.
6. B. H. Davis, Technology development for iron Fischer-Tropsch catalysts. Final Technical Report, US DOE, Contract # DE-AC22-91PC90056, 1999.
7. T. R. Motjope, H. T. Dlamini, G. R. Hearne, and N. J. Coville, Catalysis Today, 71 (2002), 335-341.
8. R. Srinivasan, R. Lin, R. L. Spicer, and B. H. Davis, Colloids and Surfaces, A: Physicochemical and Engineering Aspects, 113 (1996), 97-105.
9. R. Lin, R. L. Spicer, F. L. Tungate, and B. H. Davis, Colloids and Surfaces A: Physicochemical and Engineering Aspects, 113 (1996), 79-96.
10. C. S. Huang, B. Ganguly, G. P. Huffman, F. E. Huggins, and B. H. Davis, Fuel Science and Technology International, 11 (1993), 1289-1312.
11. M D. Shroff, D. S. Kalakkad, K. E. Coulte, S. D. Köhler, M. S. Harrington, N. B. Jackson, A. G. Sault, and A. K. Datye, Journal of Catalysis, 156 (1995), 185-207.
12. R. Zhao, J. G. Goodwin. K. Jothimurugesan, S. K. Gangwal and J. J. Spivey, Industrial & Engineering Chemistry Research, 40 (2001), 1320-1328.
13. T. F. Barton, T. Price, J. G. Dillars, Journal of Colloid and Interface Science, 141 (1991), 553-558.
14. Sarkar, U. M. Graham, J. K. Neathery, R. L. Spicer, and B. H. Davis, Abstracts of Papers, CATL-023, 231st ACS National Meeting, Atlanta, GA, United States, March 26-30, 2006.

15. R. Srinivasan, L. Xu, R. L. Spicer, F. L. Tungate and B. H. Davis, Fuel Science & Technology International, 14 (1996), 1337-1359.

Table 1. Quantitative EDS analysis of the γ – FeOOH particles after CO activation.

Element	**Weight%**	**Atomic%**	**% Uncertainty**
Carbon (Kα)	22.82	51.11	0.269
Oxygen (Kα)	9.75	16.39	0.098
Iron (Kα)	67.43	32.49	0.197

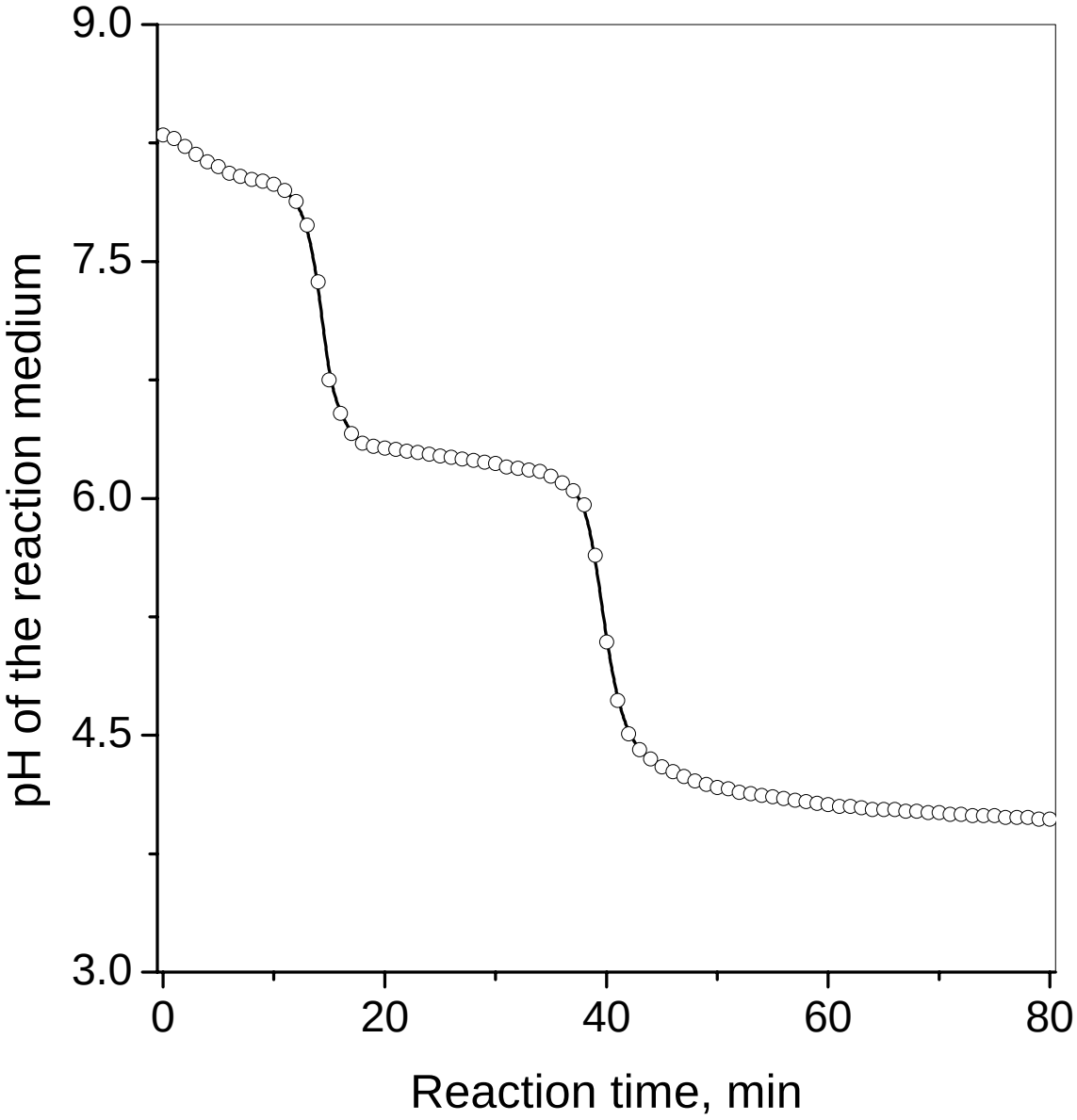

Figure 1. Variation in pH of the reaction medium with reaction time.

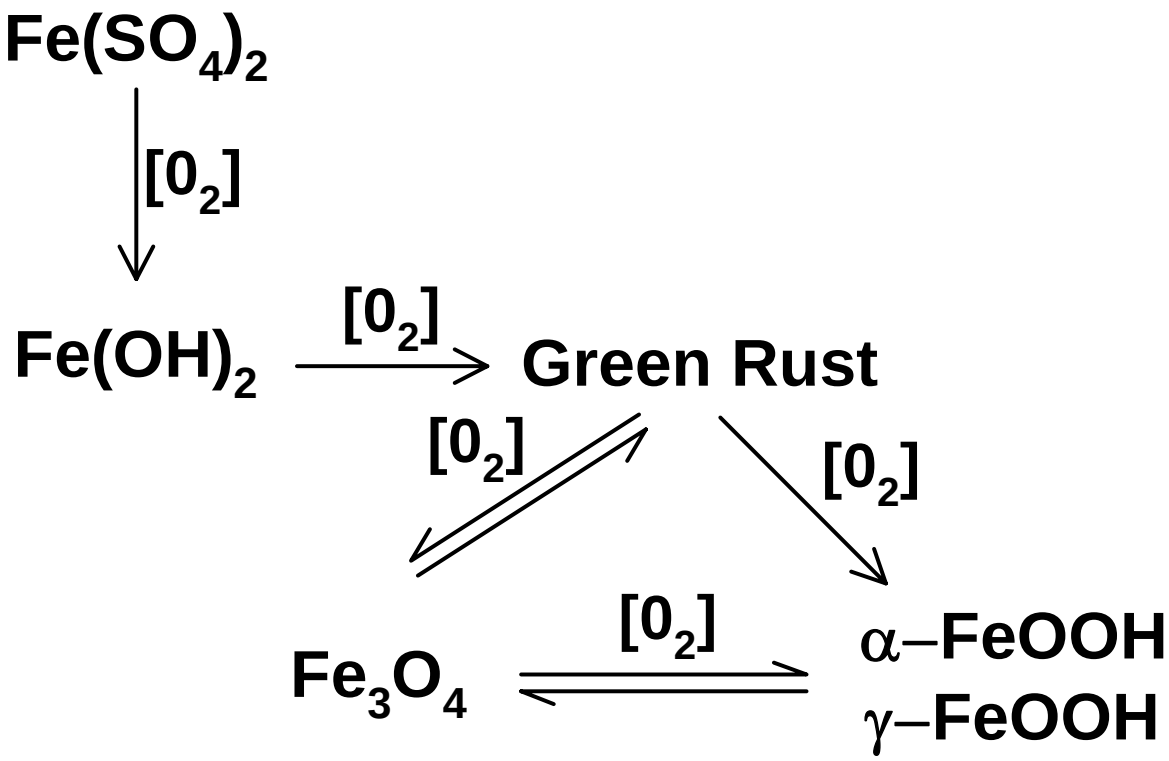

Figure 2. A pictorial reaction sequence representing the oxidation pathway from $Fe(OH)_2$ to $\gamma - FeOOH$ (Davis, 1993).

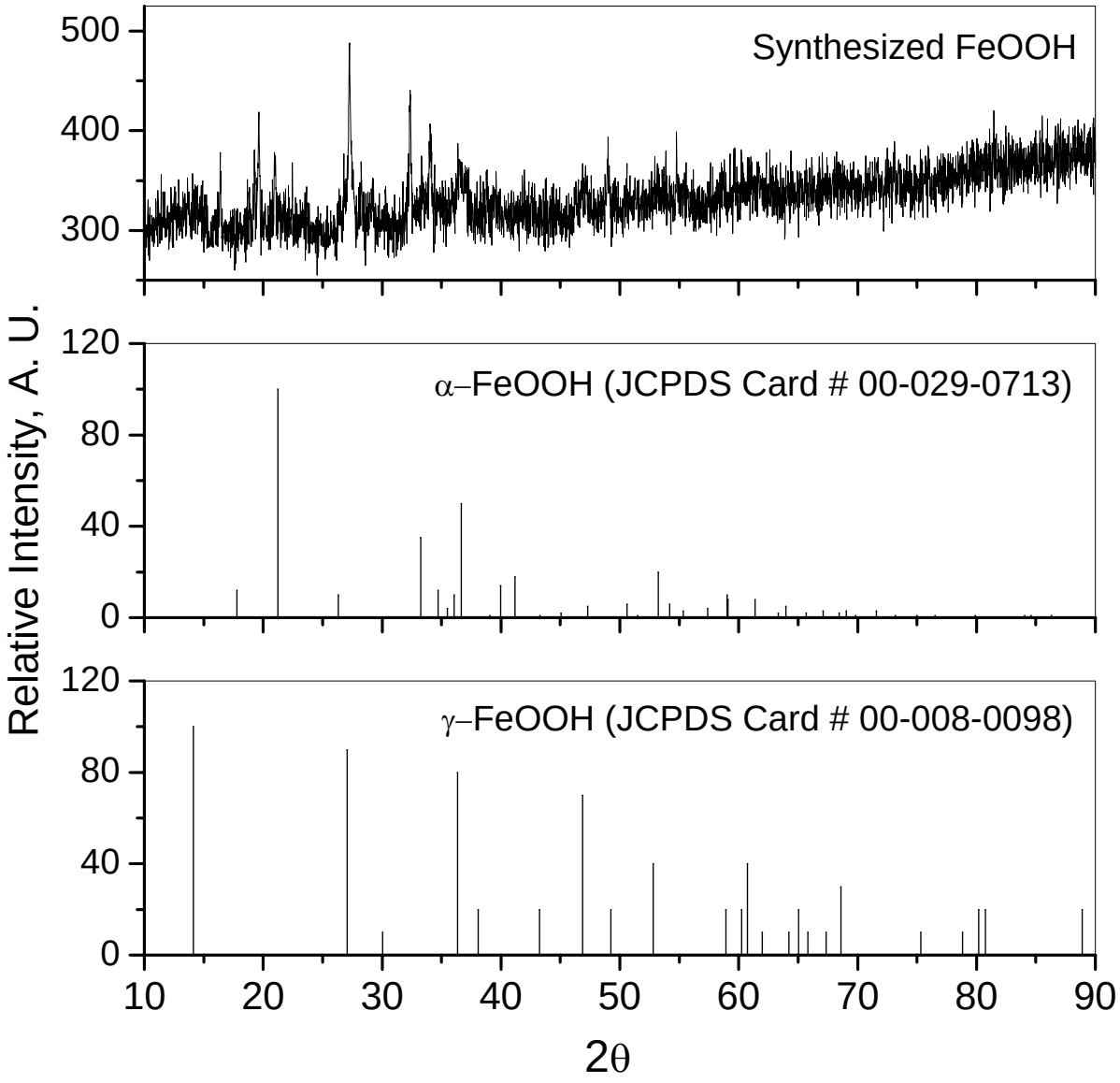

Figure 3. Powder x-ray diffraction pattern of the synthesized FeOOH and reference JCPDS pattern α – FeOOH and γ – FeOOH .

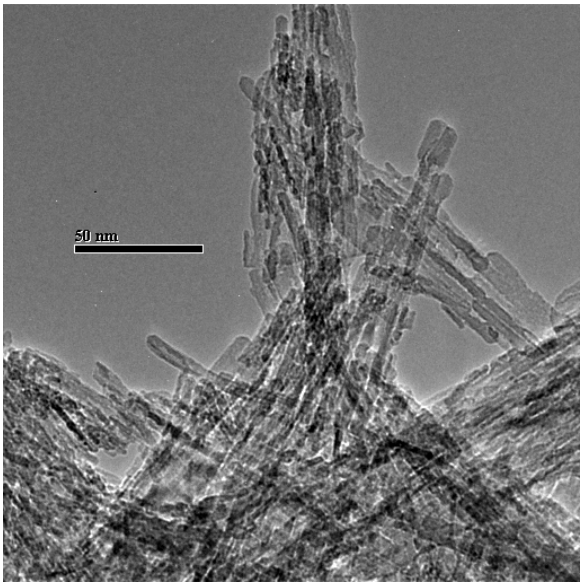

(a)

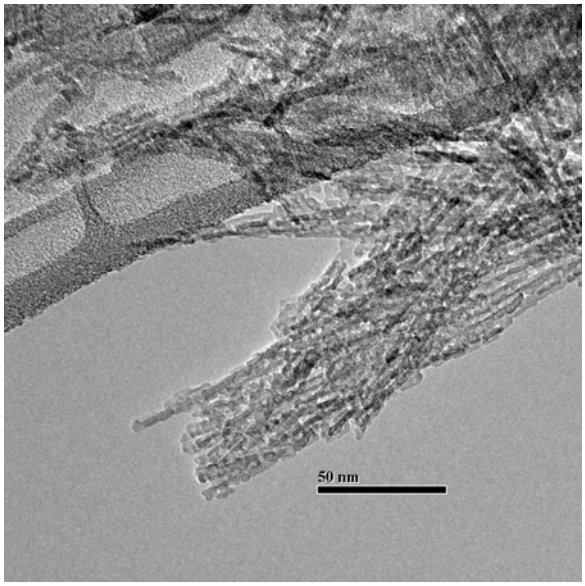

(b)

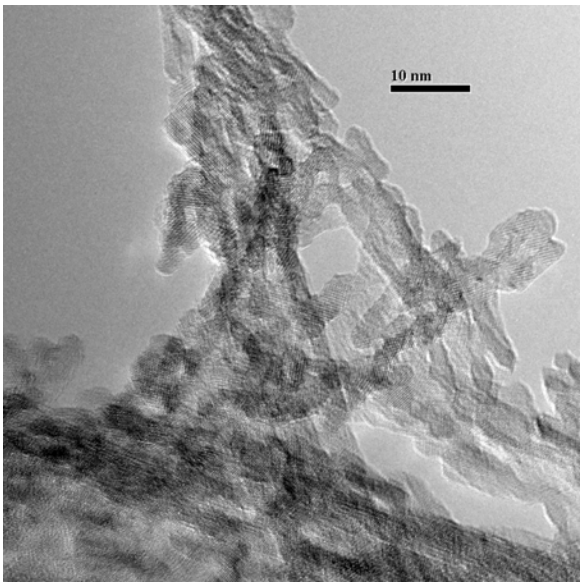

(c)

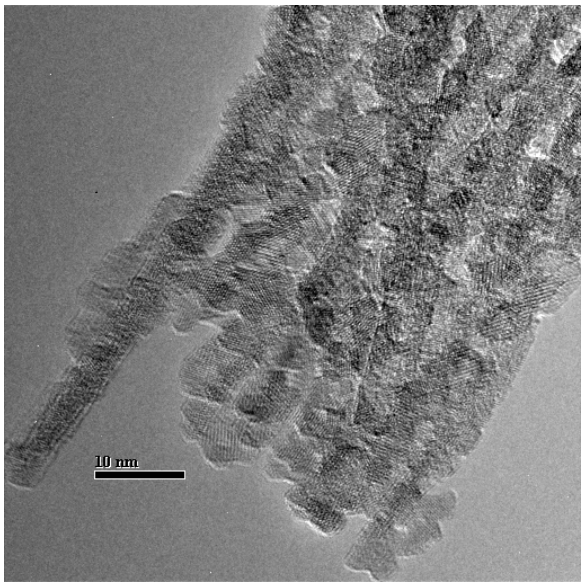

(d)

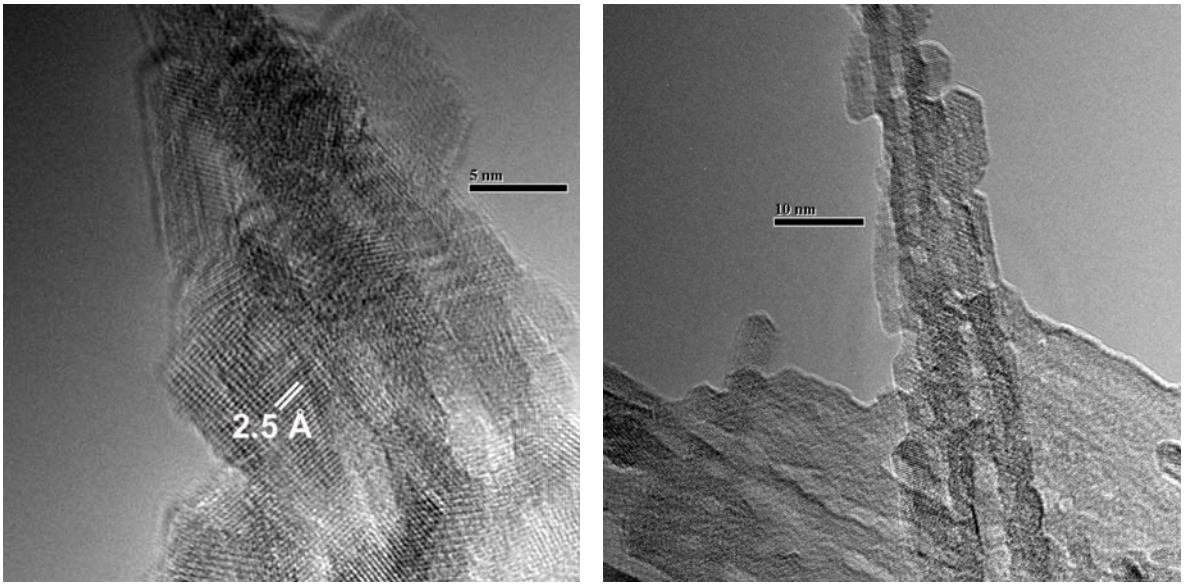

(e) (f)

Figure 4. HRTEM image of the synthesized $\gamma - FeOOH$ particles: (a) needle-shaped morphology; (b) three dimensional networks of nano-needles; (c) crystalline three dimensional structure with average diameter 5-10 nm; (d) crystalline nano-needles; (e) aggregates of nano-crystalline structure with a characteristic d-spacing of 2.5 Å; (f) crystalline nano-cylindrical structure.

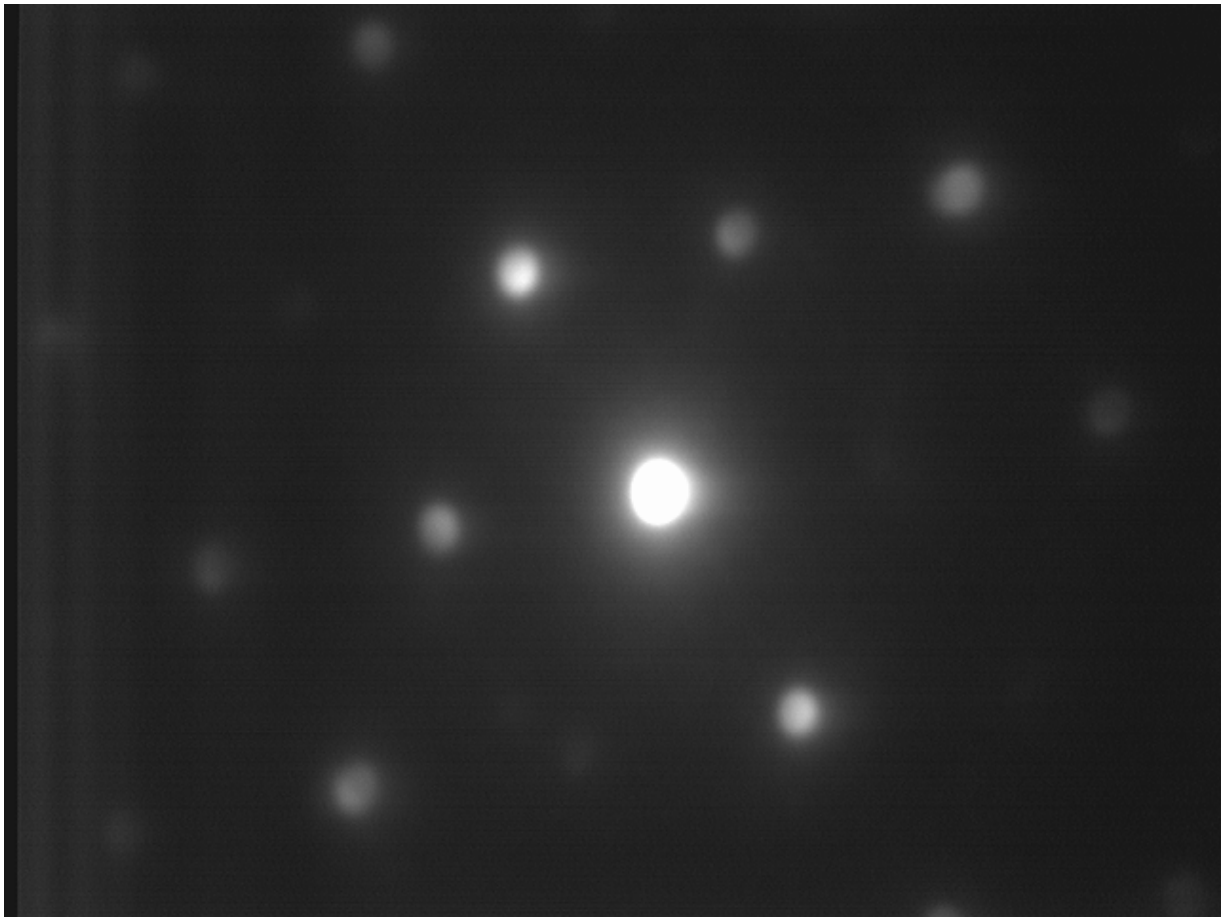

Figure 5. Electron microdiffraction pattern of the synthesized γ – FeOOH particles.

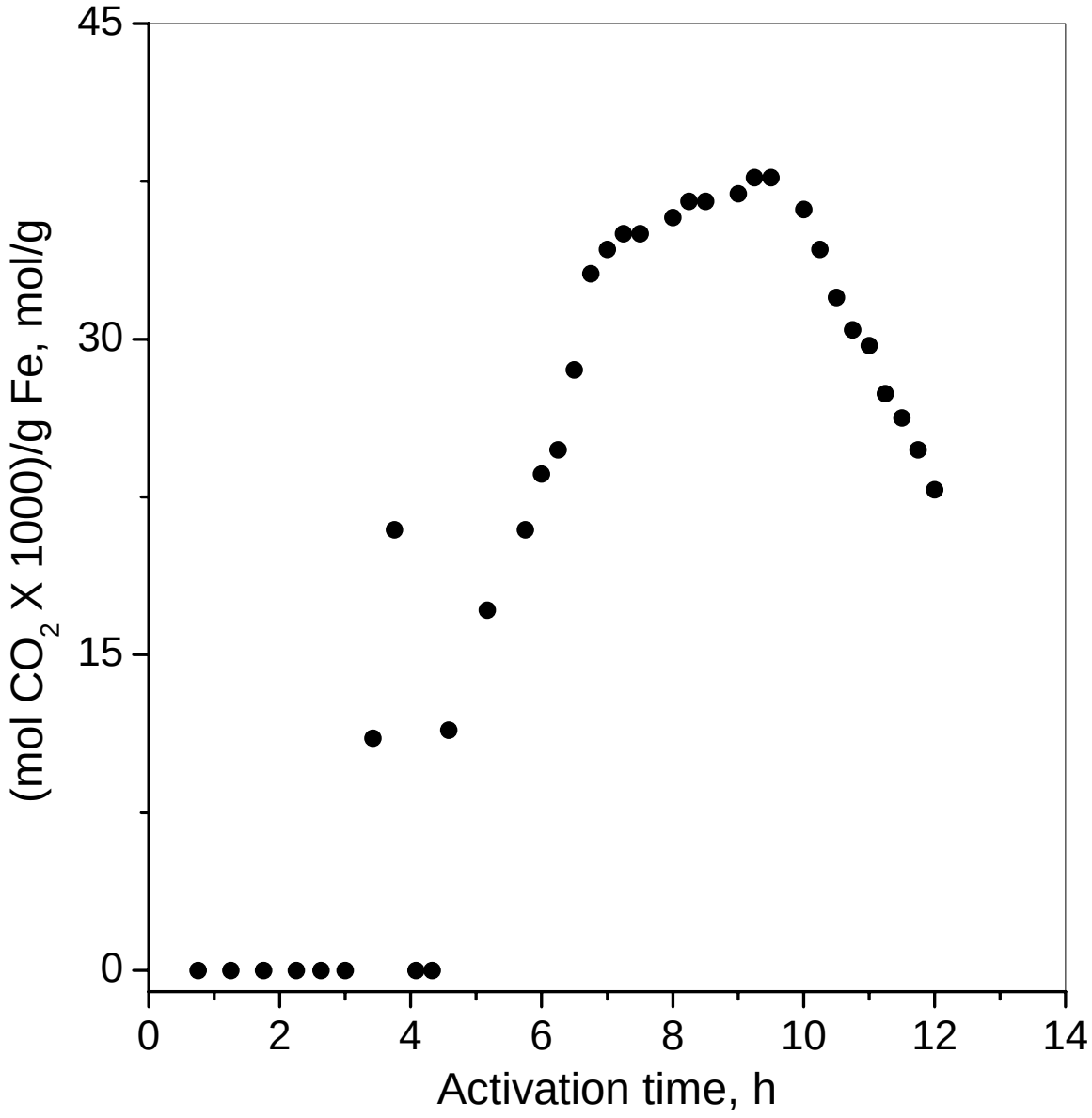

Figure 6. Variation in the amount of CO_2 generated (mol of CO_2 per g of iron) during the CO activation of the γ – FeOOH particles.

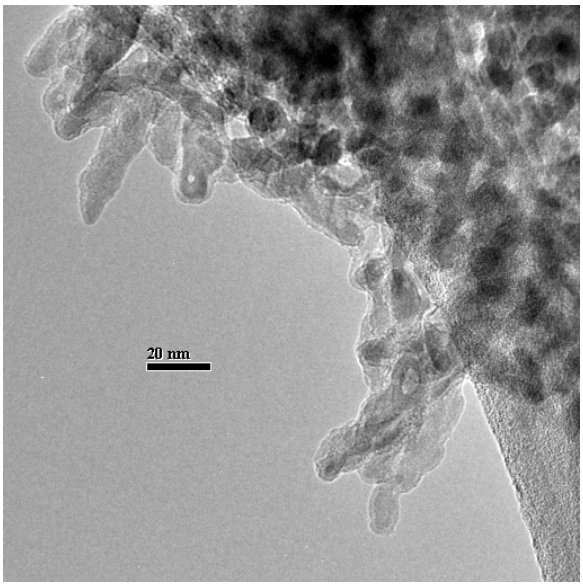

(a)

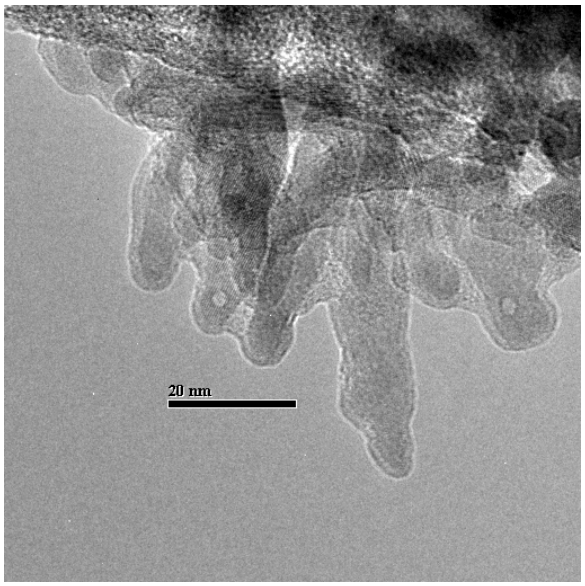

(b)

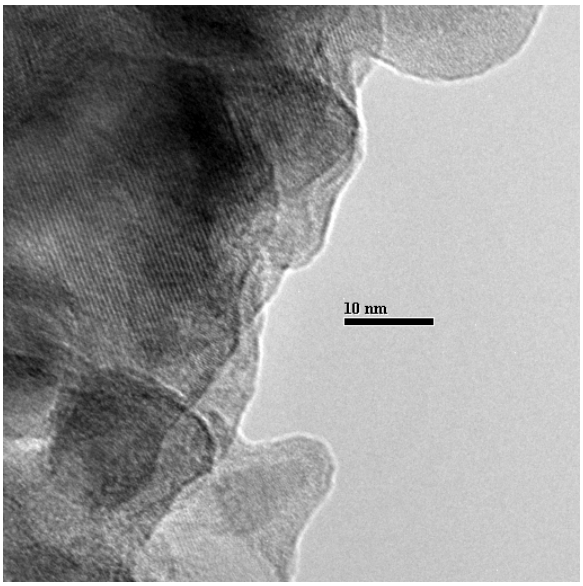

(c)

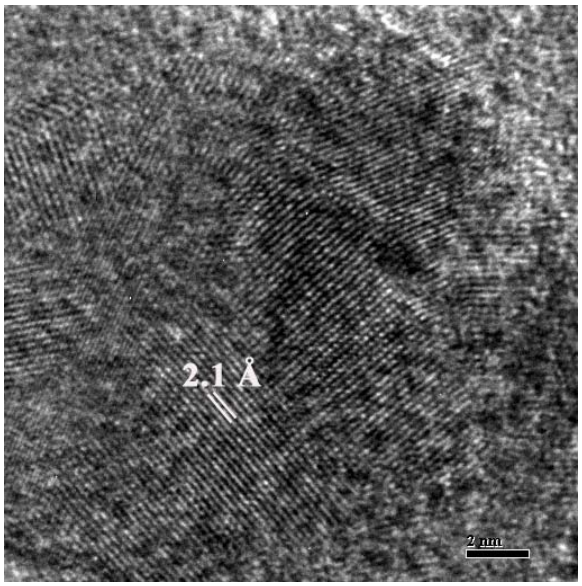

(d)

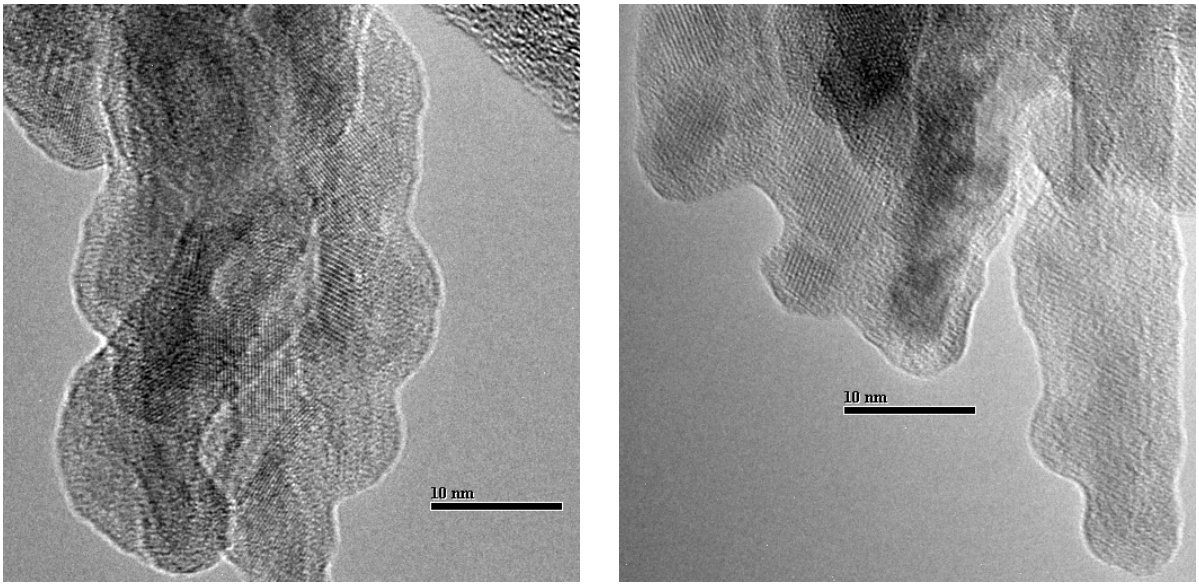

(e) (f)

Figure 7. HRTEM images of the $\gamma - FeOOH$ particles after CO activation: (a) loss of initial nano-needle like morphology on carbidation; (b) generation of non-perfect non-spherical morphology upon carbidation; (c) generation layered structure with crumpled and boulder appearance after carbidation; (d) crystalline iron carbides with a characteristic d-spacing of 2.1 Å; (e) nano-crystalline iron carbide layers; (f) aggragates of nano-crystalline iron carbides.

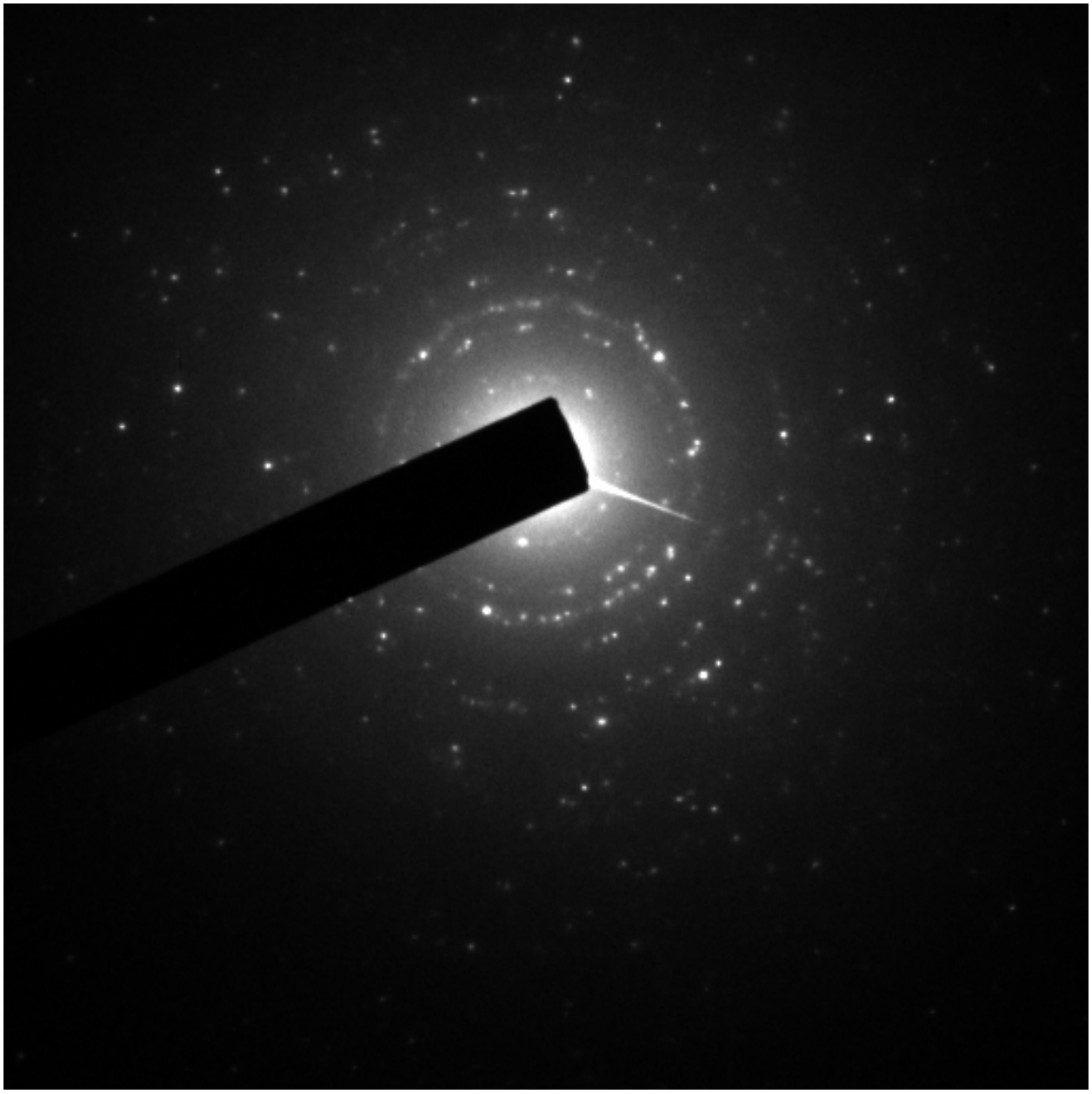

Figure 8. An electron microdiffraction pattern of the initial $\gamma - FeOOH$ particles after CO activation.

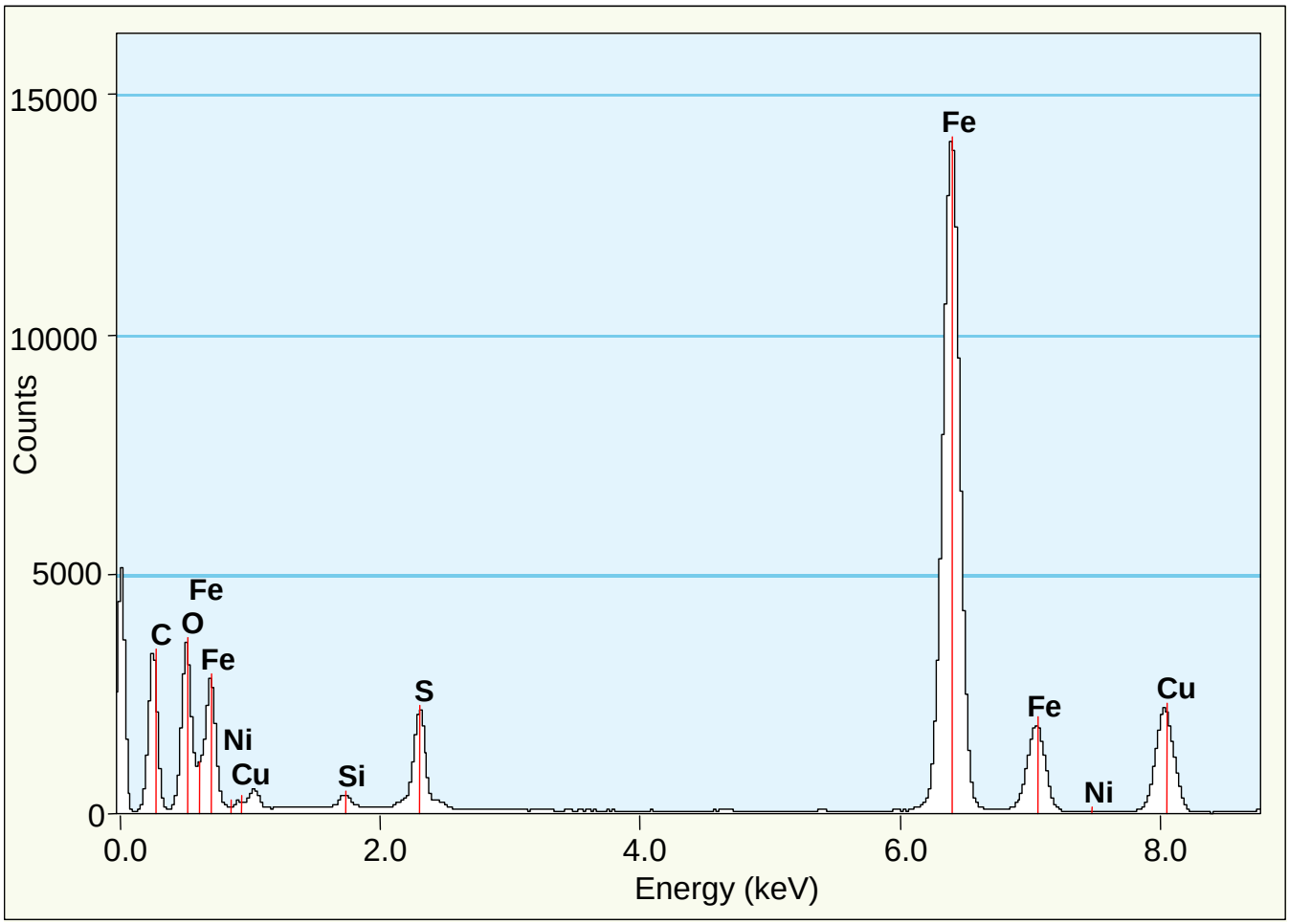

Figure 9. EDS analysis of the γ – FeOOH particles after CO activation.

Task 1.5. Development of Filter media cleaning procedure (CAER)

Subtask Completed.

Task 1.6. Chemical and physical characterization of slurry and filtrate

1. INTRODUCTION

The impact of Group 1 alkali promoters (i.e., Li, Na, K, Rb, and Cs) on the Fischer-Tropsch synthesis and water-gas shift rates and product selectivity were previously studied using a CSTR [1]. Typically, K is the promoter which offers the greatest benefit. However, rubidium, though less effective as a promoter, has an electronic transition that can be studied by EXAFS and XANES synchrotron techniques [2] and will therefore, be the focus of the current study. In our previous investigation [1], Rb was found to (1) decrease the overall CO conversion; (2) increase the deactivation rate; (3) decrease the WGS rate as a function of 1/SV; (4) improve the product selectivity by decreasing the C_2-C_4 selectivity and increasing the higher molecular weight fraction (C_5+); (5) decrease the methane selectivity; and (6) increase the C_2 olefin/paraffin selectivity.

Utilizing XANES, one goal of the current investigation was to determine the chemical compound that represents the state of the alkali promoter (in this case Rb) in the working catalyst. Also, a comparison using EXAFS, XANES, and Mossbauer spectroscopies was carried out to assess the chemical states of Fe present in the catalyst. CAER researchers visited the synchrotron at Brookhaven National Laboratory in June to assess the catalysts by XANES spectroscopy.

At the CAER, catalysts were directly retrieved from the CSTR and cooled under inert conditions in the wax to solidify the catalyst particles in the waxy matrix to prevent contact with the atmosphere. This was accomplished one of two ways - by stopping the reactor at the end of the run or by use of a dip tube to remove catalyst during on-stream testing.

2.1 CATALYST PREPARATION

A well-studied iron catalyst was split into two separate batches and promoted with Rb using rubidium carbonate as the precursor at two levels: 1.44/100 and 5.0/100 Rb to Fe atomic ratio. These catalysts are designated as catalysts 1.44RbC and 5RbC, respectively. The two loadings were used, because it was difficult to assess whether or not the Rb signal would be observed by X-ray absorption spectroscopies in the lower loaded catalyst. In addition, a 5.0/100 Rb to Fe atomic ratio catalyst was also prepared using rubidium nitrate instead as the precursor. The catalyst is designated as 5RbN. The "C" and "N" designations refer to the precursor, either carbonate or nitrate, respectively. The original precipitated iron catalyst was prepared with tetraethyl orthosilicate, iron nitrate, potassium carbonate and copper nitrate. Ferric nitrate solution was first prepared by dissolving $Fe(NO_3)_3$ in distilled and deionized water, and the amount of orthosilicate needed to make Si:Fe of 4.6 was added. The mixture was stirred vigorously until the tetraethyl orthosilicate was hydrolyzed. Tetraethyl orthosilicate and iron nitrate mixture was then added to a CSTR precipitator vessel together with ammonium hydroxide. By maintaining the slurry pH at 9 and an average residence time of 6 minutes, a base catalyst material with an iron to silicon molar ratio of 100:4.6 was obtained. The slurry was then filtered with a vacuum drum filter and washed twice with deionized water. The final

filtration cake was dried in an oven with flowing air at 110°C for 24 hours. The catalyst was crushed and calcined in a 350 °C oven under an air flow for 4 hours. Rubidium was added to obtain a promoter to iron atomic ratio of either 1.44/100 or 5.00/100. The catalyst was dried at 110°C overnight with good mixing following the impregnation of the Rb precursor.

EXPERIMENTAL

2.3 X-RAY ABSORPTION NEAR EDGE AND EXTENDED X-RAY ABSORPTION FINE STRUCTURE SPECTROSCOPIES

XANES studies were carried out at the K-edge of Fe for catalysts 1.44RbC and 5RbC, as well as reference materials, including an Fe metallic foil, Fe_2O_3, Fe_3O_4, and an Fe-carbide reference material prepared at the CAER previously verified by XRD. XANES spectra were also recorded at the K-edge of Rb for catalysts 1.44RbC and 5RbC after 180 h reaction, and for catalyst 5RbN directly after activation and after 25 h of FT reaction. In addition, spectra were recorded for two Rb oxide reference materials, a rubidium hydroxide material, and a rubidium carbonate reference. X-ray absorption near edge spectroscopy measurements on references and catalyst samples were conducted at the National Synchrotron Light Source (NSLS) at Brookhaven National Laboratory (BNL), using beamline X18b equipped with a Si(111) channel cut monochromator. A crystal detuning procedure was employed to prevent glitches arising from harmonics. The second crystal of the channel cut monochrorly linked to the crystal and slightly spring loaded. The other side is a picomotor, a very fine high pitch screw that turns by piezo, which allows for slight detuning of the crystal. The X-ray ring at the NSLS has a flux of 1E10 photons per second at 100 mA and 2.5 GeV, and the energy range capability

at X18b is 5.8-40 keV. As previously reported, the catalysts were previously run in the CSTR until steady state conversion was achieved. The catalyst samples were suspended in the waxy FT matrix for analysis. XANES data were recorded near the Rb K-edge after cooling under He flow to liquid N_2 temperatures. To obtain a second Rb oxide reference, RbOH was heated to 275^{o}C in flowing helium and held for 20 min at that condition prior to cooling to LN conditions.

Data reduction of the XANES spectra was carried out with WinXAS (5). Standard data reduction was carried out by pre-edge background removal and normalization by division of the height of the absorption edge. Previously, in the case of Fe K-edge results, linear combination fitting of the experimental catalysts with select references was carried out using WinXAS over the energy range of 7.1 to 7.16 keV for Fe. For the case of Rb K-edge results, the catalysts were compared to references over the range 15.15 to 15.25 keV. However, a linear combination fitting procedure was not necessary.

2.4 REACTION TESTING

In-situ catalyst activation

Iron catalysts must be activated with either H_2, CO or synthesis gas. Activation procedures can have a significant effect on the selectivity and activity of iron-based catalysts. It was reported that catalysts activated with CO yielded higher long-chain hydrocarbons than syngas and H_2-activated catalysts. In addition, activation conditions may also influence the performance of the iron catalyst. In this study, the promoted iron catalysts were pretreated with CO at 270^{o}C, 1.2 MPa for 24 hours.

For the 1.44RbC and 5RbC separate catalyst tests, the reactor was loaded with 40.0 g of Rb-promoted catalyst. The initial conditions for the reactor were 175 psig,

270°C, with the traps at 200, 100, and 0 °C. The feed gas was initially set to 72.0 slph with a composition of 40% H_2 and 60% CO for a H_2:CO ratio of 0.67 and WHSV of 3. 180.0 g of the startup oil C-30 was used. The catalyst was pretreated with CO at 270 ° C for 24 hours. After the CO conversion stabilized, the catalyst was run for approximately 180 hours, at which point the run was stopped, and the catalyst retrieved, solidified in the waxy matrix to allow for spectroscopic characterization in the in-situ state.

DISCUSSION

Figure 1 shows the XANES spectra taken at the Rb K-edge. This includes a comparison of the catalysts 5RbN prepared using the nitrate precursor with 5RbC and 1.44RbC prepared from the carbonate precursor, and various reference materials, including RbOH, Rb_2CO_3, and two different Rb_2O references, one that was purchased, and one prepared from the in-situ decomposition of RbOH at 275°C in helium flow. The reason the RbOH decomposition was carried out was due to reported problems with the differentiation of Rb compounds in earlier studies by Davis and coworkers [2]. An overlay of all catalyst samples with the Rb_2CO_3 reference indicate very strongly that the active state of the Rb promoter is an oxidized state of +1, and that the chemical species present in the working catalyst is likely rubidium carbonate. It is not clear at this time if the rubidium carbonate is the actual promoter for FT selectivity, or if the rubidium carbonate is a spectator and that there is a different surface species in close contact with iron carbides that is responsible for promoting effect, as has been suggested by some in the case of K [3]. However, it is notable that decreasing the Rb content from 5.0/100 to 1.44/100 Rb to Fe atomic ratio did not lead to a significant change in the XANES white line shape or intensity to signify that a different chemical state of Rb was present.

REFERENCES

1. W. Ngantsoue-Hoc, Y. Zhang, R.J. O'Brien, M. Luo, and B.H. Davis, Appl. Catal. 236 (2002) 77.

2. E. J. Doskocil, S. V. Bordawekar and R. J. Davis, J. Catal. 169 (1997) 327.

3. S. Li, S. Krishnamoorthy, A. Li, G.D. Meitzner, E. Iglesia, J. Catal. 206 (2002) 202.

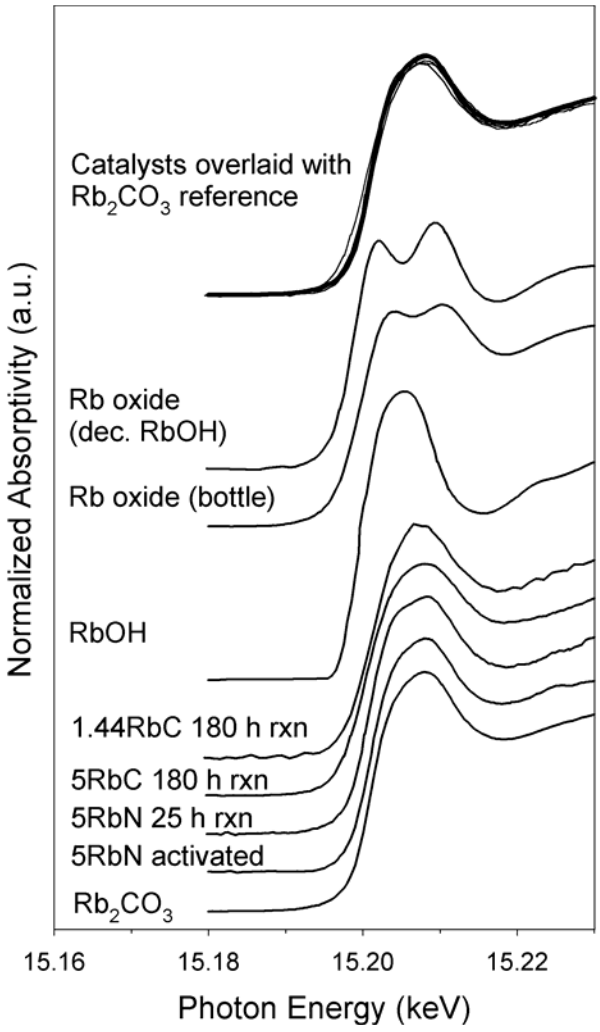

Figure 1: Rb K-edge results. XANES spectra of, moving upward, (a) Rb_2CO_3 reference, (b) the activated 5RbN catalyst, (c) the activated 5RbN catalyst after 25 h onstream, (d) the activated 5RbC catalyst after 180 h onstream, (e) the 1.44 RbC catalyst after 180 h onstream, (f) an Rb_2O sample purchased, (g) an Rb_2O sample prepared from the decomposition of RbOH in helium at 275^{o}C, and (h) an overlay of all the catalyst samples with the Rb_2CO_3 reference.

Task 2. Phase II Bubble Column Pilot Plant Studies

INTRODUCTION

In the second phase of the current program, a pilot-scale SBCR system was integrated with a filtration scheme developed in Phase I. In Phase I, filtration properties of various iron-based catalyst slurries were correlated with the chemical and physical changes occurring during activation and FTS synthesis. Our research has focused on understanding the phase changes during activation/reduction and their associated effects on filtration properties. Additionally, cleaning/flux maintenance procedures were optimized for the various filter media types test in the research program.

In the beginning of this research program, our objective was to develop a single-stage filtration scheme that would produce a wax with clarity of less than 5 ppm. Based on our operating experience and analytical information gathered with the pilot filtration rig in Phase I, this objective was overly optimistic in hindsight. A two-stage system is required because of the combined stresses of catalyst loading and the formation of nano-scale carbide particles formed during activation and synthesis. Additionally, the fouling rate of the filter media is directly proportional to catalyst slurry concentration; thus, a primary separation stage would have the potential to lower the stress on the filtration membrane.

In Phase II, our objective is to address the technical barriers associated with integrating an improved filtration strategy into commercial FTS unit. A series of pilot plant runs will obtain all the necessary data needed for the F-T filter system scale-up.

Laboratory evaluations will also be used to support the pilot tests as well as help to optimize both the F-T catalyst and the overall process.

Work has been completed to modify the CAER's 4 liter bubble column reactor to include the FT wax filtration scheme developed during the previous Phase of this research program. In the modified reactor system, a moyno-type progressive cavity pump will be included to convert the reactor from a natural to forced circulation liquid circuit. The wax/catalyst slurry will have two separate flow paths: 1. a low flow circuit (1-2 lpm) passing through the bubble column, and 2. a higher rate slurry path through the cross-flow filter.

EXPERIMENTAL

Integrated SBCR Two-Stage Filtration Apparatus

In the current configuration, the bubble column has a 5.08 cm diameter and a 2 m height with an effective reactor volume of 3.7 liters; a simplified schematic of the SBCR system is shown in Figure 1. The synthesis gas passes continuously through the reactor and is distributed by a sparger near the bottom of the reactor vessel. The product gas and slurry exit the top of the reactor and pass through an overhead receiver vessel where the slurry disengages from the gas-phase. Vapor products and unreacted syngas exit the overhead separator vessel, enter a warm trap (333 K) followed by a cold trap (273 K). A dry flow meter down stream of the cold trap measures the exit gas flow rate.

A downcomer tube, descending from the overhead separator, carries the F-T catalyst slurry to the suction side of a moyno-type progressive cavity pump. The slurry is discharged from the pump to a primary separation device (an inertial separator similar to a hydroclone to lower the catalyst concentration to about 0.5 wt%). From the bottom of

the primary separator, a catalyst-rich stream will be recycled to the reactor vessel while the lean catalyst/slurry stream will be diverted to a filtration circulation loop.

The flow rate of catalyst-rich slurry to the reactor will be controlled manually (1-3 lpm) by adjusting a throttle valve connected to the bottom of the primary separator such that the catalyst is well-dispersed in the SBCR. The filtration loop flow rate will be measured by a non-intrusive coriolis flow meter. A detailed schematic of the filtration and reactor piping is shown in Figure 2. Quantifying the flow will be important because the slurry axial velocity is crucial in cross-flow filtration. The flow rate of slurry to the reactor will be measured indirectly by difference by temporarily cutting off the flow to the reactor and measuring the flow increase in the filtration loop. Since the slurry pump is a positive displacement device (i.e., no slurry slippage inside the pump), the total flow should remain the same regardless of pressure changes incurred by the temporary switching of the reactor circuit.

Polishing of the clarified slurry will be by a cross-flow filter element similar to the type supplied by Pall Filtration in Phase I. The filters' stainless steel membranes have a nominal pore size of 0.1 μm. The surface of the filter media substrate is coated with a proprietary sub-micron layer of zirconia. Ideally, the axial velocity through the crossflow unit should be greater than 4 m/s to minimize the boundary layer of particles near the membrane surface.

The filter assembly is configured such that the filter media could be replaced on-line, without aborting or interrupting the reactor run. The flux of the clean permeate through the cross-flow unit wax will be controlled by the pressure in the let-down vessel or hot trap. Therefore, the trans-membrane pressure (TMP) will be fixed for a given

filtration event. The TMP can be changed manually varying the set point of the pressure regulator connected to the let-down vessel. The flux rate is measured by weighing the mass of permeate collected in the collection vessel hot trap.

A filtration event is initiated by the overhead vessel level controller. The wax permeate flow from the filter will be switched on by a control valve between the permeate discharge of the cross-flow unit and the collection vessel. Hence, a relatively constant inventory of slurry will be maintained within the SBCR system as long as the superficial gas velocity remains constant. Changes in the gas hold-up due to a variable gas velocity will need to be calculated so that the space velocity can be accurately quantified.

The level or volume of the slurry within the overhead receiver is continuously monitored by measuring the differential pressure across the height of the vessel. Argon is purged through each of the pressure legs to keep the lines free of slurry. Slurry volume within the receiver is controlled to be no more than 1.3 liters by removing wax from the reactor system via the level control valve.

Continuous Filtration Platform

Filtration Test Platform. An existing pilot plant platform was modified into a crossflow filtration test unit. This unit, depicted schematically in Figure 3, will allow several types of crossflow filter media to be researched under simulated FTS conditions. Three prototype filtration modules were received from Pall, Inc. The modules have an inlet (filtrate) and outlet (retentate) ports with ½" tubing ends, and a permeate port, located near the midpoint of the unit. The filters' stainless steel membranes have a nominal pore

size of 0.1 μm. The surface of the filter media substrate is coated with a proprietary sub-micron layer of zirconia.

The filtration piping and instrumentation is heated via several circuits of copper heat-trace tubing. A Therminol 66 heat transfer fluid is circulated through the heat-trace tubing using an electrically-heated hot oil system. The temperature controller was calibrated to operate over a temperature range of 180 to 250 ^{o}C.

Data gathering and process control functions are accomplished by a National Instruments real-time computer system. A 98 liter (26 gallon) slurry mixing tank is heated by hot-oil circulation jacket. Slurry mixtures of catalyst and wax are loaded batch-wise into the system. A Liberty Process Equipment (progressive cavity) pump is used to circulate the mixture through the crossflow filter element. A manually-actuated valve, located downstream of the filter element, maintains a slurry flow rate set-point of 2 to 40 lpm.

Unfiltered slurry (or retentate) passing through the filter tube is recycled to the mixing tank. The differential pressure across the filter medium or trans-membrane pressure (TMP) is automatically controlled by a let-down valve. The permeate can be recycled to the slurry tank for continuous filtration simulation (in order to maintain a constant solids concentration in the system) or can be collected and removed from the system to test semi-batch filtration schemes. The permeation rate is periodically measured by diverting the stream into a collection flask over a convenient time interval. Samples can be collected before the filter for characterization. In tests where the catalyst is activated, a gas pad of CO or syngas can be applied to the system otherwise the system vapor space is purged with inert gas such as argon or nitrogen. Slurry temperature,

simulating the FTS activation conditions, can be controlled up to 240 ^{o}C. Modular filtration media can be tested under various filtration rates, differential pressures and operating modes. The system is designed so that the filter unit can be bypassed in order to change filters while the slurry continues recirculation.

Filter Flux maintenance System. The flux maintenance system is capable of back flushing the membrane with a piston pump that is triggered by a computer controlled timer. The back-flush fluid consists of cleaned permeate stored in a 40 ml tube bomb located near the suction side of the piston pump. However, backflushing with clean permeate is only used as a last resort. Preferably, the maintenance procedure is to turn off the permeate flow on a short but regular period. This system will be used throughout the study to develop an optimum cleaning program that can sustain a permeate flux rate over a many days.

RESULTS

During the start-up of the modified SBCR/Filtration system, several problems were encountered with the pump used to circulate the wax/catalyst slurry though the cross-flow filter element and reactor. The pump, manufactured by Liberty, is a moyno-type progressive cavity design capable of delivering 20 lpm of FT slurry at 230 ^{o}C. The unit has a stainless steel rotor with an elastomeric stator designed for pumping slurries at FT synthesis and activation conditions.

Initially, the as-received pump could not pass a 13.8 bar (200 psig) static pressure test at ambient temperature. Consequently, the pump was returned to the manufacturer for extensive seal modifications. Upon receiving the modified pump, the unit was placed

into service for a “hot” shakedown test with Durasyn oil at pressure (175 psig). The modified seal continued to leak at a small and acceptable rate in the order of 1 g/min. However, leak problems were encountered in the threaded seal of the stator and the pump housing. The stator was resealed with a thick Teflon tape and a high-temperature pipe sealant which initially slowed the total system leaks to less than 50 g/hr.

At this point, the system was tested with catalyst at activation and synthesis gas, in the hopes that the seal leak rates would be impeded by the presence of small catalyst particles. During the activation of the catalyst with elevated temperature (> 270 ^{o}C) the elastomer pump stator released sulfur compounds thereby totally deactivating the iron-based catalyst. Additionally, difficulties in maintaining an acceptable leak rate from the pump seal and stator housing continued after an exhaustive effort of implementing counter measures. Consequently, the system leak rate always exceeded the expected production rate of wax; therefore, no online filtration could be accomplished.

In order to test the filtration scheme during a long-term test, the filtration system was operated independent of the SBCR pilot system in the continuous filtration plant at low pressure (1.7 bar at the pump discharge). In lieu of FT wax produced directly from the bubble column, we prepared a test slurry batch containing FT wax obtained from previous pilot SBCR and CSTR reactor tests and activated ulrafine Mach I iron catalyst (0.26 wt% as raw catalyst). The molecular weight distribution of the composite wax is shown in Figure 4. The goal of this test was to monitor and record filter flux measurements over a long term time on stream period (500+ hours). Various flux maintenance or filter cleaning procedures were employed over the long term test, attempting to stabilize the flux over time.

Long Term Filtration Run with Mach I FT Composite Wax.

Various flux maintenance or filter cleaning procedures were employed over the long term test, attempting to stabilize the flux over time. These studies examined flux values for the 26" filter with a media area of 0.0198 m^2 (0.213 ft^2) a slurry density of approximately 0.69 g/cm^3 at 200^oC, a Mach-1 catalyst concentration of 0.26 wt%, 17 kg (37.5 lbs) of FTS wax, and a TMP of 1.4 bar (20 psid). The filtration process was run in a recycle mode, whereas clean permeate was added back to the slurry mixture, thus allowing the catalyst concentration to remain approximately constant over the course of the run (given minor adjustments for ~5 ml permeate and slurry samples taken throughout the test).

Initial flux readings decreased dramatically as a mass transfer boundary layer formed on the filter media. This boundary layer appears to remain somewhat constant after about 6 hours online, whereas the slope of the flux versus time graph (Figure 5) becomes fairly linear. This linear decrease in flux continues over the next 43 hours. This could be attributed to fouling of the membrane by the small iron/iron carbide particles.

At this point, a passive flux maintenance procedure was employed (49.33 hours TOS), introducing a 30 second flux shut-off period every 30 minutes. This allowed the catalyst slurry to recirculate through the filter with no radial permeate flow through the filter membrane. This axial flow is designed to relax the filter membrane, possibly releasing any embedded particles and aiding in increasing the flux. The flux did not initially increase significantly after the TMP was reinstated to 1.4 bar. It did however, slowly increase after a few of the back pulse cycles were able to have an effect on the

filter membrane. After 12 of the 30 second back pulse cycles (~6 hours), the flux increased 161% overall (from 0.5 to 1.3 lpm/m^2 or 17.6 to 46.0 GPD/ft^2). Thereafter the flux slowly decreased over the next 280 hours, down to 0.76 lpm/m^2 or 27.0 GPD/ft^2 (a 41.3% loss in flux over that span).

An active flux maintenance procedure was initiated at this point, beginning with a 2 second back flush of clean permeate through the filter membrane. Again, this flux maintenance cycle was continued every 30 minutes for just over 24 hours. The flux initially recovered to 0.90 lpm/m^2 (32.0 GPD/ft^2), but fell again within 24 hours to baseline value of 0.76 lpm/m^2 (26.7 GPD/ft^2) without including clean permeate backflush. The flux maintenance was again returned to passive flux maintenance (no backpulse with clean permeate), only increasing the flux off time to 60 seconds every 30 minutes. Thereafter, the flux steadily decreased over the next 120 hours from 0.77 to 0.58 lpm/m^2 (27.3 to 20.4 GPD/ft^2). At 480 hours online a 1 hour flux off cycle was attempted, increasing the flux back to 0.62 lpm/m^2 (29.1 GPD/ft^2), a 42.6% increase. The flux off cycle was then returned to the 60 second off cycle for the next 48 hours, once again showing a flux decrease to 0.62 lpm/m^2 (21.9 GPD/ft^2). Another 1 hour flux off cycle returned the flux to 0.72 lpm/m^2 (25.3 GPD/ft^2 only a 15.5% increase). The next 23 hours using a 1 minute flux off cycle every 30 minutes showed a much more slight decrease in flux (down to 0.65 lpm/m^2 or 23.1 GPD/ft^2). A final 1 hour flux off cycle showed minimal flux increase (0.04 lpm/m^2 or 5.6%).

In Figure 6, the Fe content of both the slurry and permeate samples is displayed versus the time-on-stream. The permeate purity was consistently below 35 ppm (as Fe) for the entire run with over 85% below 16 ppm level. The variation over iron content

could be due to sampling during or after flux maintenance events which can disturb the boundary layer of submicron particles on the membrane surface.

At about 560 hours online the flux was shut off for the overnight period to clean the filter for a flux versus TMP test. The flux versus TMP test (see Figure 7) indicated a rather linear relationship between the two variables, with the highest flux (0.85 lpm/m^2 or 29.9 GPD/ft^2) obtained at the upper end of the TMP range 1.72 bar (25 psid).

CONCLUSIONS

A successful filtration demonstration run using a mixture of FT wax and an ultra-fine starting catalyst was completed. For the most part, the target purity level of less than 15 ppm iron was attained in the final wax products. A simple flux maintenance procedure of interrupting the permeate flow for 30 seconds per half hour was effective in recovering the initial membrane fouling; however, the long-term steady-state flux was not achieved with the method. Flux stability was attained only after increasing the permeate off cycle to 1 hour per day in addition to 30 seconds off per half hour cycle.

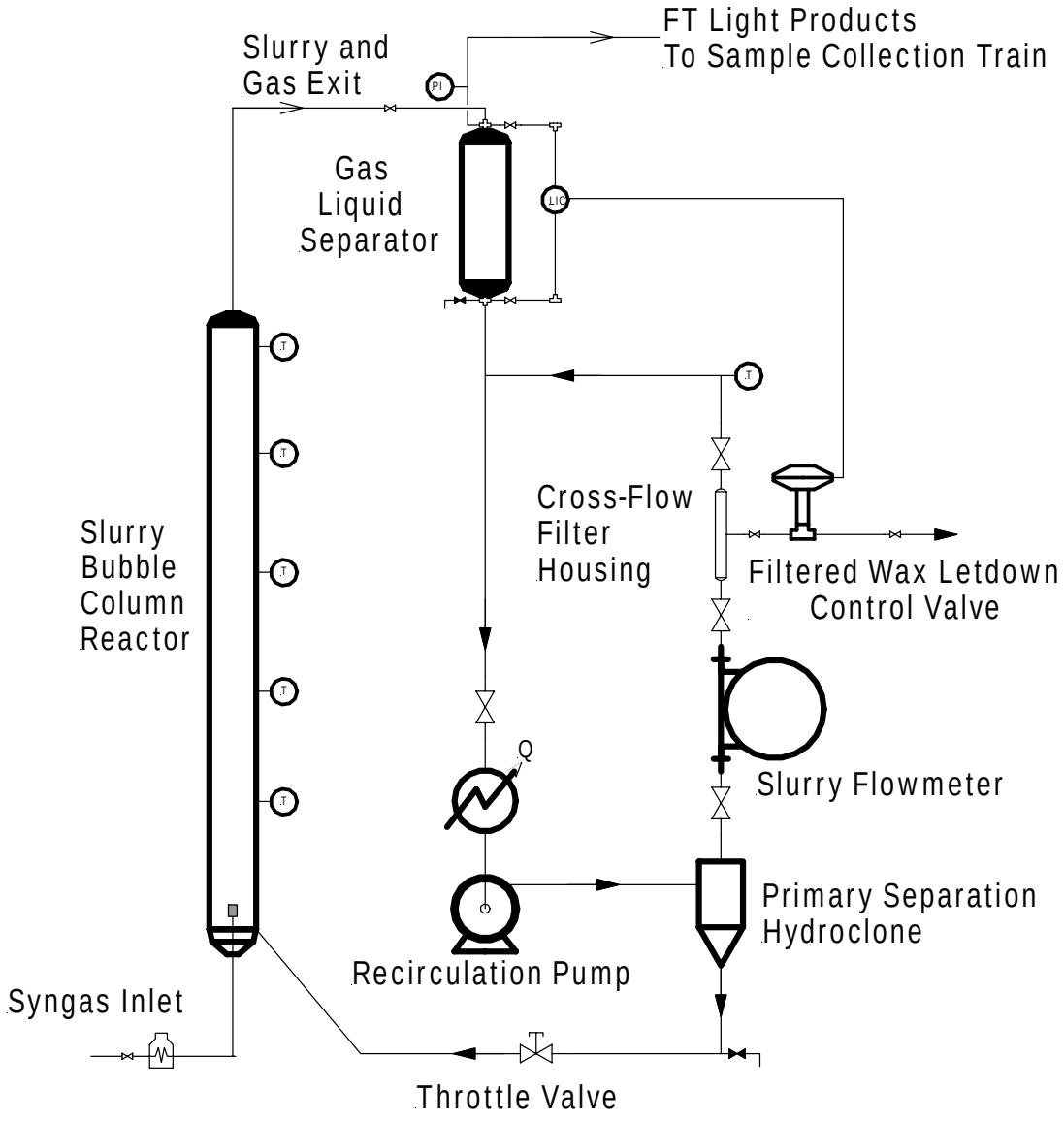

Figure 1. Schematic of the SBCR and Filtration System

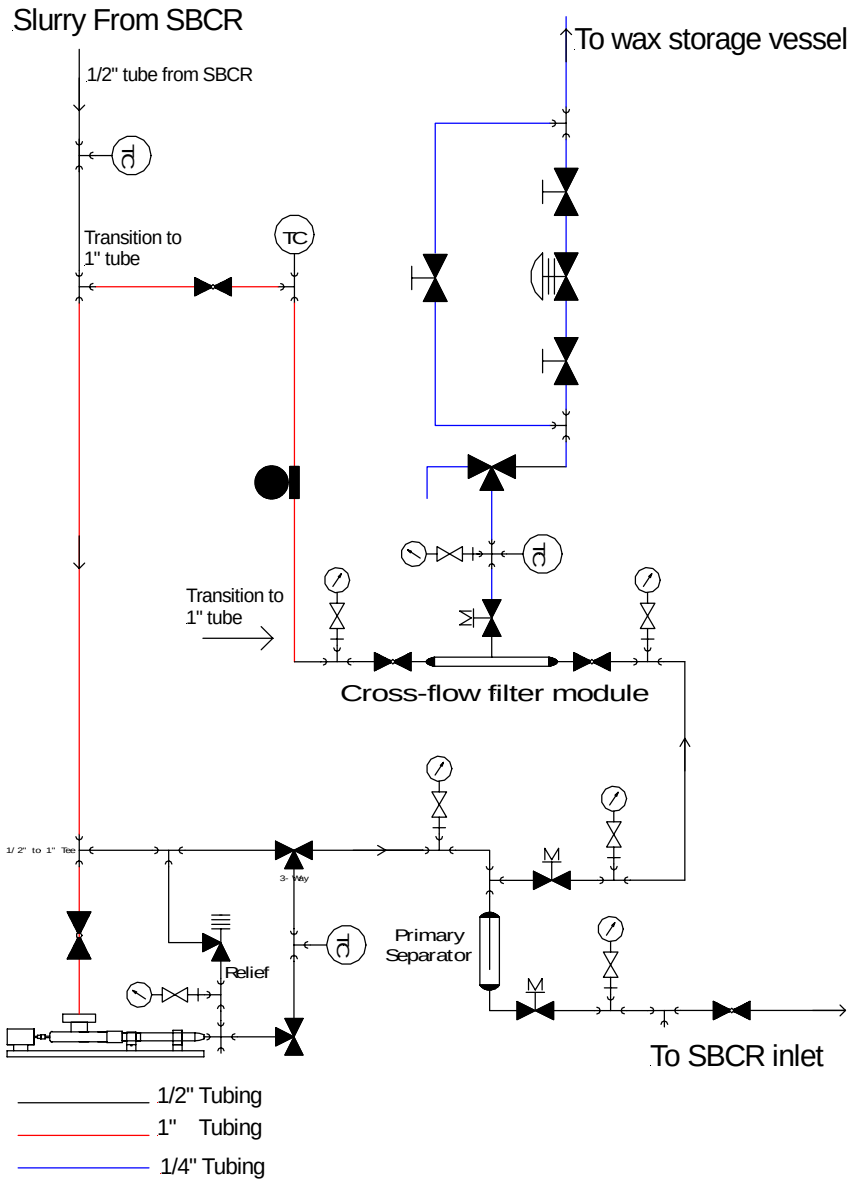

Figure 2. Piping Diagram Detail of the SBCR Filtration Loop.

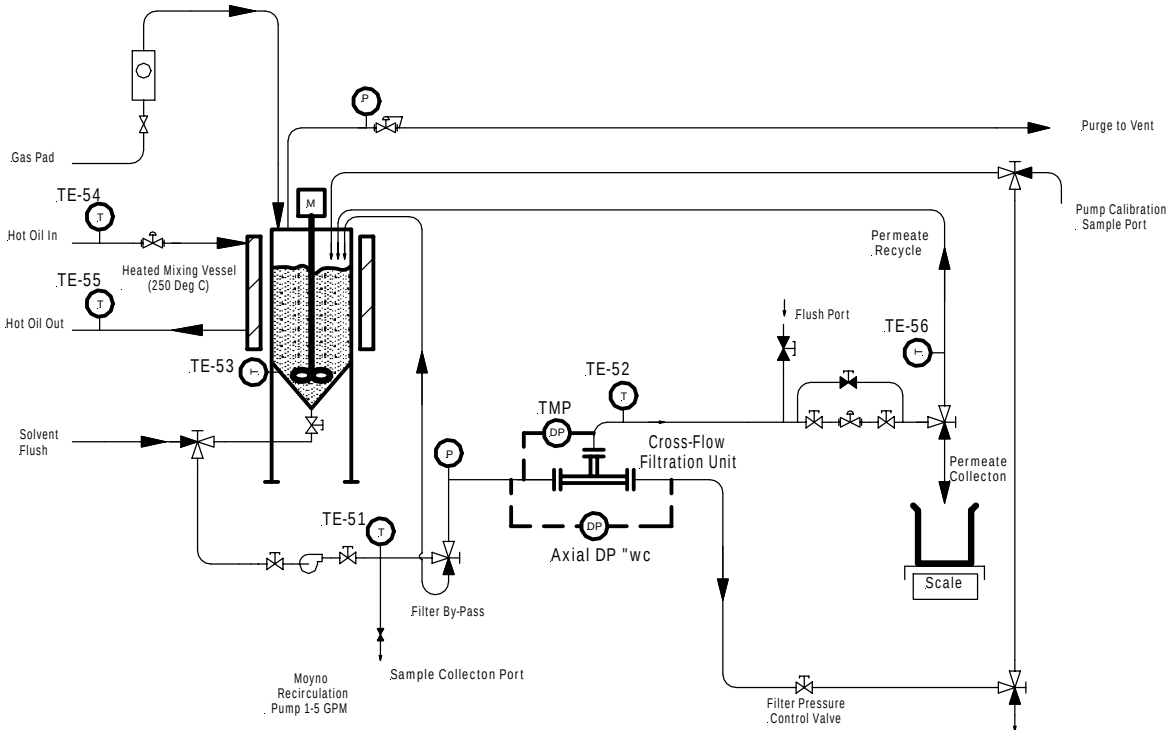

Figure 3. Schematic of the filtration test platform.

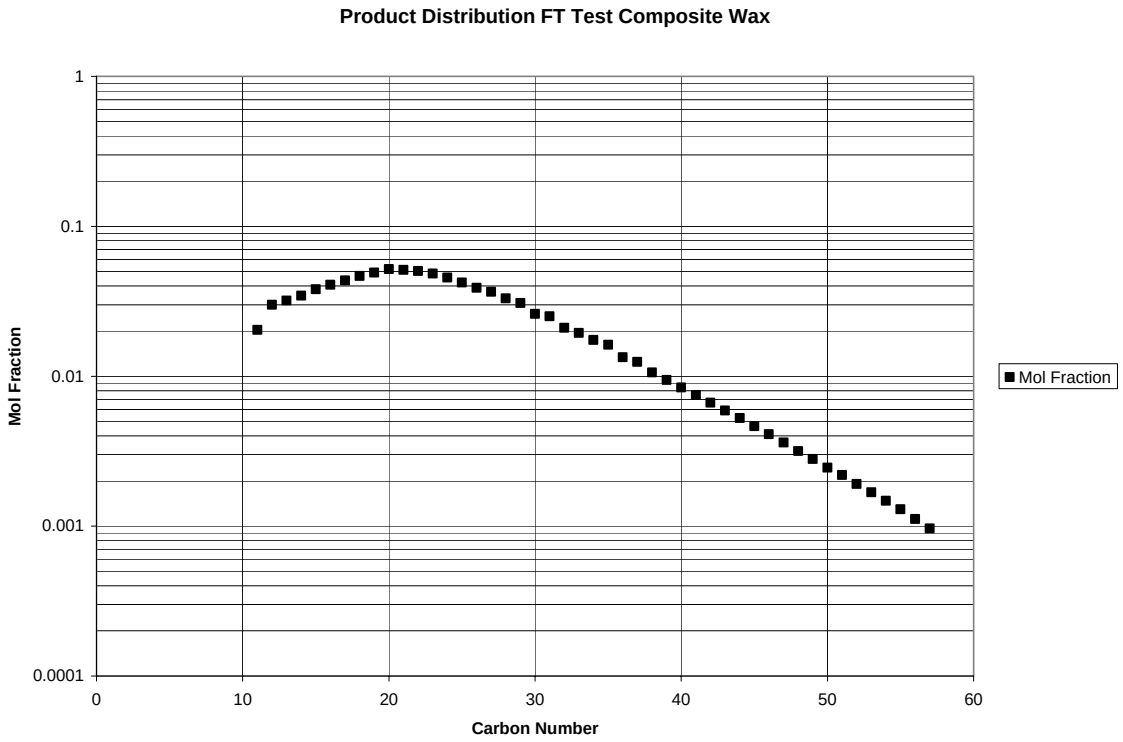

Figure 4. Product Distribution of the Composite FT Wax Used in the Long-term Filtration Run

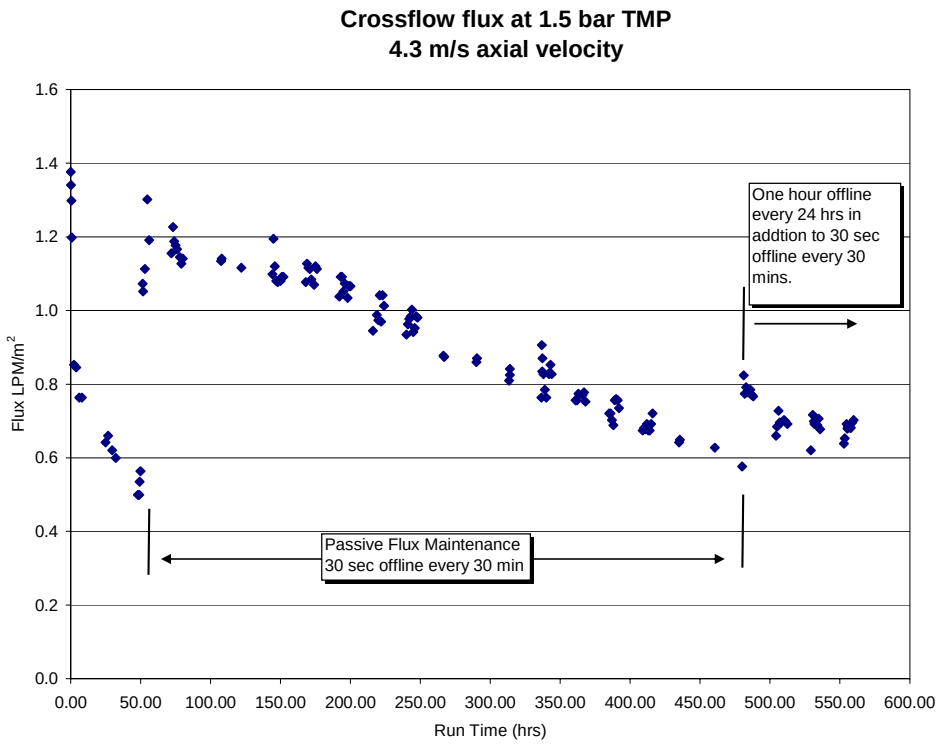

Figure 5. Permeate Flux vs. Time On Stream

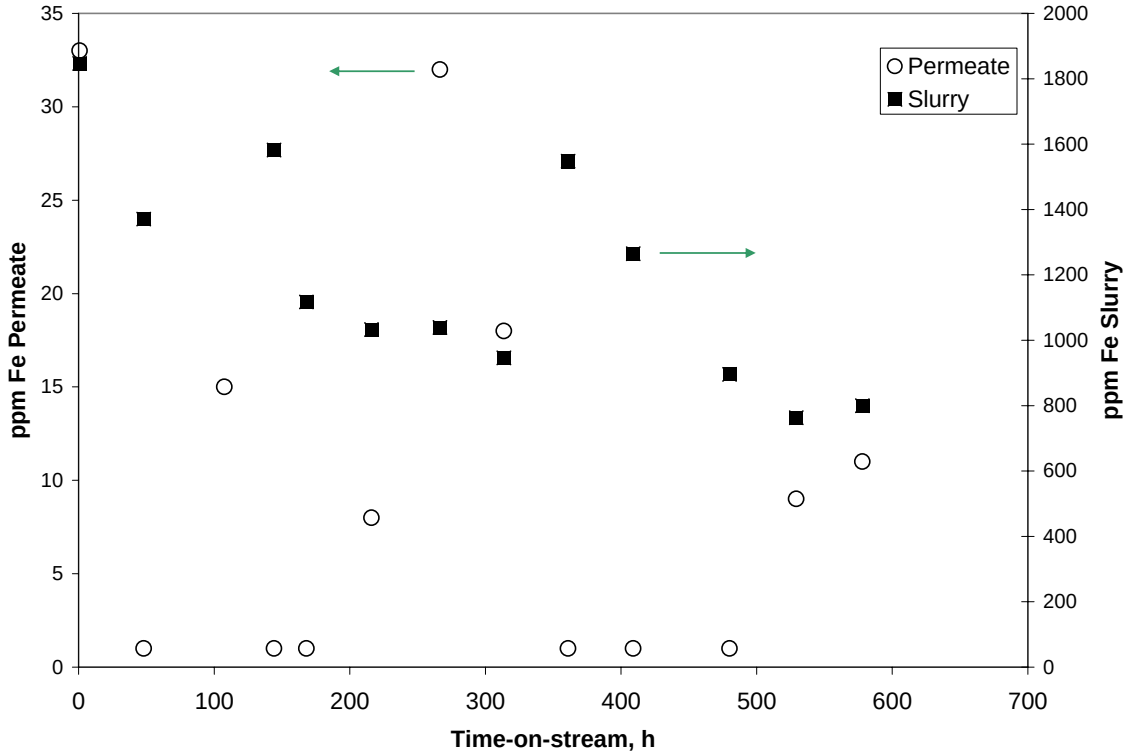

Figure 6. Filtration Pilot Demonstration Run: Iron Content of Slurry and Permeate Samples vs. TOS

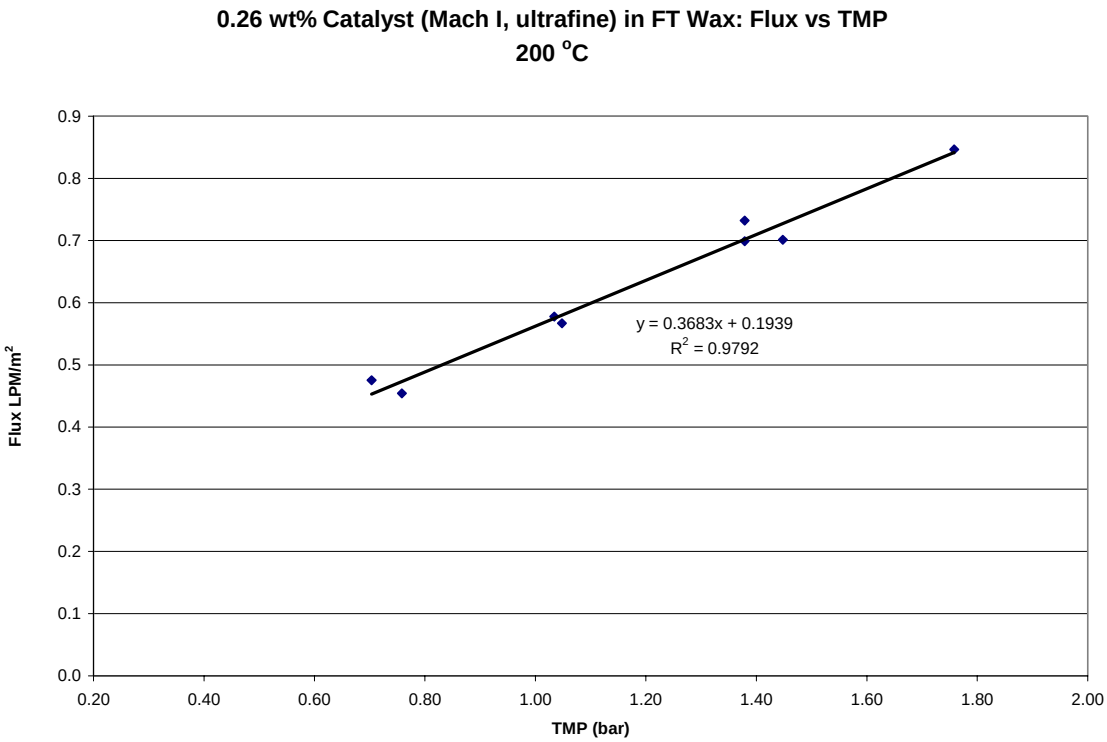

Figure 7. Permeate Flux vs. Trans-Membrane Pressure: Data taken at the end-of-run with over 500 hours TOS.

PATENTS, PRESENTATIONS AND PUBLICATIONS

2006 Publications

1. Jacobs, G.; Ricote, S.; and Davis, B.H.; "Low temperature water-gas shift: type and loading of metal impacts decomposition and hydrogen exchange rates of pseudo-stabilized formate over metal/ceria catalysts," Applied Catalysis A: General 302 (2006) 14.

2. Sparks, D.E.; Patterson, P.M.; Jacobs, G.; Crocker, M.; and Chaney, J.A.; "Supported bismuth oxide catalysts for the selective reduction of NO with propene in lean conditions," Catalysis Communications 7 (2006) 122.

3. Ricote, S.; Jacobs, G.; Milling, M.; Ji, Y.; Patterson, P.M.; and Davis, B.H.; "Low temperature water-gas shift: characterization and testing of binary mixed oxides of ceria and zirconia promoted with Pt," Applied Catalysis A: General 303 (2006) 35.

4. Sparks, D.E.; Patterson, P.M.; Jacobs, G.; Dogimont, N.; Tackett, A.; Crocker, M.; "Bi_2O_3/Al_2O_3 catalysts for the selective reduction of NO with hydrocarbons in lean conditions," Applied Catalysis B: Environmental 65 (2006) 44.

5. Ji, Y.; Toops, T.J.; Graham, U.M.; Jacobs, G.; Crocker, M.; "A kinetic and DRIFTS study of supported Pt catalysts for NO oxidation," Catal. Lett. 110 (2006) 29.

6. Keane, M.A; Jacobs, G.; Patterson, P.M., "Ni/SiO_2 promoted growth of carbon nanofibers from chlorobenzene: characterization of the metal sites," J. Colloid Interface Sci. 302 (2006) 576.

7. Jacobs, G.; Keogh, R.A.; Davis, B.H., "Steam Reforming of Ethanol over Pt/Ceria with co-fed Hydrogen, J. Catal., accepted, in press.

8. Book chapter - Das, T.K.; Conner, W.A.; Jacobs, G.; Zhan, X.; Li, J.; Dry, M.E.; and Davis, B.H.; "Fischer-Tropsch Synthesis: Kinetics and Effect of Water for a Co/Al_2O_3 Catalyst," in press.

9. Book chapter - Jacobs, G.; Das, T.K.; Li, J.; Luo, M.; Patterson, P.M.; and Davis, B.H., "Fischer-Tropsch synthesis: influence of support on the impact of co-fed water for cobalt-based catalysts," in press.

Presentations

Jacobs, G.; Das, T.K.; Li, J; Patterson, P.M.; Luo, M.; Davis, B.H. "Fischer-Tropsch Synthesis: Impact of water on the activity and lifetime of cobalt catalysts," 10th International Symposium on Catalyst Deactivation, Feb 3-7, Berlin, Germany, 2006.

Jacobs, G.; Ricote, S.; Ji, Y.; Patterson, P.M., Davis, B.H., “Metal Promoted Binary Oxides of Ceria and Zirconia for Low Temperature Water-Gas Shift”, AICHE Spring National Meeting, April 23-27, 2006.

Luo, M., Jacobs, G., and Davis, B.H., “Overview of Fischer-Tropsch Products and Their Upgrading to Useful Products.”, AICHE Spring National Meeting, April 23-27, 2006.

Jacobs, G.; Pigos, J.M., Brooks, C.J., Graham, U.M., Davis, B.H., "Recent developments in metal/oxide low temperature water-gas shift catalysts for fuel processor applications", Tri-State Catalysis Society Symposium, Sept. 13, Lexington, KY, 2006.

Pigos, J.M. Brooks, C.J., Jacobs, G., Davis, B.H., “Evidence of enhanced LTS water-gas shift rate with sodium promoted Pt-ZrO_2-based catalyst discovered by combinatorial methods,” AIChE Annual Meeting (2006).

Pigos, J.M., Brooks, C.J., Jacobs, G., Davis, B.H., “DRIFTS studies of platinum-based zirconia catalyst promoted with sodium discovered by combinatorial methods,” Prepr. Am. Chem. Soc. Div. Pet. Chem. (2006).

Other Travel

Jacobs, G. and Ji, Y., Brookhaven National Laboratory, June 15 - 19, 2006.

Patents Issued 2006

N/A